Geometrical Improvement of Fuel Nozzle Locations in the SGT-750 Gas Turbine

An investigation into fuel-air mixing in main channels 1 & 2

Aryan Delir

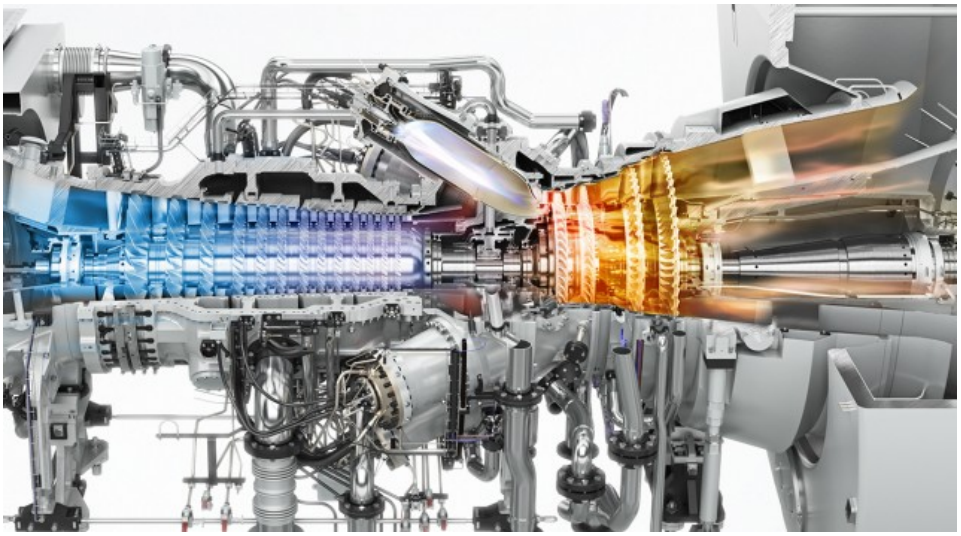

Linköpings universitet
Institutionen för ekonomisk och industriell utveckling
Examensarbete 2022|LIU-IEI-TEK-A–22/04487–SE

Linköpings universitet
Institutionen för ekonomisk och industriell utveckling
Ämnesområdet Mekanisk värmeteori och strömningslära
Examensarbete 2022|LIU-IEI-TEK-A–22/04487–SE

Geometrical Improvement of Fuel Nozzle Locations in the SGT-750 Gas Turbine

An investigation into fuel-air mixing in main channels 1 & 2

Aryan Delir

Academic supervisor: Anton Persson
Industrial supervisor: Daniel Lörstad
Examiner: Joakim Wren

LINKÖPINGS UNIVERSITET

Linköping universitet
SE-581 83 Linköping, Sverige
013-28 10 00, www.liu.se

Abstract

This study was conducted on SGT-750, which utilizes can type fourth generation DLE burner, developed at Siemens Energy AB, in Finspång, Sweden. The aim of this study is to obtain a flat fuel profile at the outlet of main channel 1 and main channel 2, demonstrating a proper mixing of fuel and air in the main channels leading to reducing local high-temperature points, and thus, reducing thermal NOx emissions. Furthermore, it is of prime importance to minimize fuel concentrations near the walls of the main channels to decrease laminar flame speed, such that if highly reactive fuels are used, the risk of flashbacks into the burner is eliminated. STAR-CCM+ is the software used for CFD simulations, and Design Manager is used for sweeping the location of fuel nozzles tangentially. Firstly, three grids are generated for the grid independence study with four, nine, and sixteen million cells. The parameters of interest for this evaluation are the mass flow rate and standard deviation of equivalence ratio, as well as velocity and fuel profiles at the outlet of main channels 1 and 2. It is found that the grid with nine million cells has an acceptable balance between the computational costs and the accuracy required. Moreover, the grid independence study revealed that as the grid becomes finer, tangential average of equivalence ratio is lower at the low radius and higher at the high radius. Thereafter, with the proper choice of the grid, three turbulence models namely, k-ε Realizable, k-ε Lag EB, and k-ω SST have been used to find the most stable RANS turbulence model to minimize the risk of non-convergence issues during design iterations in the improvement phase. It is depicted that the k-ε Realizable is the most stable RANS model among the models tested for this case, and this model is used for further improvements on the location of fuel nozzles. Ultimately three design improvements have been presented for both main channels based on dividing the outlet plane into four parts and minimizing the difference between the tangential average of equivalence ratio for the two middle portions and minimizing the tangential average of equivalence ratio for the near wall portions. It is demonstrated that design 3 is the best choice for main channel 1 due to lower fuel concentrations near the wall and flat fuel profile in the middle of the channel. However, for main channel 2, it was noticed that the Baseline Design is the best choice when non-highly reactive fuels are used, while Design 3 is most suitable for highly reactive fuels.

Acknowledgements

This thesis work has been conducted at Siemens Energy AB, in Sweden. Therefore, I want to sincerely thank all the people who contributed to the accomplishment of this thesis work, especially my industrial supervisor, Daniel Lörstad who unconditionally helped and guided me throughout the project. I also want to thank my manager Saeid Kharazmi for giving me the opportunity to work on this exciting project. I also want to thank my academic supervisor Anton Persson for his continuous support, as well as my examiner Joakim Wren for providing helpful feedback. I want to dedicate special thanks to my family for their unconditional love and support. Mom, Dad, and Arad, I know this means something to you too. Last but not least, I want to thank my friends for life, Korren. You make me laugh, you let me cry, and you are the reason this thesis took seven months to write. Vi ses i dimman.

Aryan Delir, Linköping, August 2022

Nomenclature

Abbreviations and Acronyms

Abbreviation	Meaning
Avg	Average
CFD	Computational Fluid Dynamics
CH_4	Methane
CO	Carbon Monoxide
D	Dimension
DLE	Dry Low Emission
DNS	Direct Numerical Simulation
ER	Equivalence Ratio
FDM	Finite Difference Method
FEM	Finite Element Method
FGM	Flamelet Generated Manifold
FVM	Finite Volume Method
GTE	Gas Turbine Engine
H	Hydrogen
HVAC	Heating, Ventilation, and Air Conditioning
ICE	Internal Combustion Engine
kg	Kilogram
km	Kilometer
Lag EB	Lag Elliptic Blending
LES	Large Eddy Simulation
LiU	Linköping University
LPM	Lean Premixed
MW	Megawatt
N	Nitrogen
NO	Nitrogen Monoxide
NO_2	Nitrogen Dioxide
NOx	Nitrogen Oxides
O	Oxygen
O_3	Ozone
OH	Hydroxyl
ppm	Parts Per Million
RANS	Reynolds Average Navier-Stokes
RAS	Reynolds Average Simulation
Re	Reynolds Number
RPL	Rich-Pilot-Lean
RST	Reacting Species Transport
s/sec	Seconds
SDER	Standard Deviation of Equivalence Ratio
SST	Shear Stress Transport
STAL	Svenska Turbinfabriks Aktiebolaget Ljungström
Tan	Tangential

Abbreviation	Meaning
TKE	Turbulent Kinetic Energy
UHC	Unburned Hydrocarbons
URANS	Unsteady Reynolds Average Navier-Stokes
WLE	Wet Low Emission

Latin Symbols

Symbol	Description	Units
C_v	Specific Heat at Constant Volume	$\left[Jkg^{-1}K^{-1}\right]$
C_μ	Turbulent Viscosity	$\left[kgm^{-1}s^{-1}\right]$
c	Progress Variable	$[-]$
E	Total energy per Unit Volume	$\left[Jm^{-3}\right]$
F	Force	$[N]$
f_b	Body Force	$[N]$
I	Identity Matrix	$[-]$
i	Internal Energy	$[J]$
k	Turbulent Kinetic Energy	$\left[m^2s^{-2}\right]$
P	Pressure	$[Pa]$
$\overline{P}$	Pressure Tensor	$[Pa]$
q	Heat Flux	$\left[Jm^{-2}\right]$
R	Specific Gas Constant	$\left[JK^{-1}kg^{-1}\right]$
S	Strain Rate Tensor	$\left[s^{-1}\right]$
S_E	Energy Source Term Per Unit Volume	$\left[Jm^{-3}\right]$
T	Temperature	$[K]$
$\bar{T}$	Viscous Stress Tensor	$[Pa]$
T_{RANS}	Average Reynolds Stress Tensor	$\left[kgs^{-1}s^{-2}\right]$
t	Time	$[s]$
U	Velocity Vector	$\left[ms^{-1}\right]$
u	Velocity Component in X Direction	$\left[ms^{-1}\right]$
u^+	Non-dimensional Tangential Velocity	$[-]$
v	Velocity Component in Y Direction	$\left[ms^{-1}\right]$
w	Velocity Component in Z Direction	$\left[ms^{-1}\right]$
y^+	Non-dimensional Wall Distance	$[-]$
Z	Mixture Fraction	$[-]$

Greek Symbols

Symbol	Description	Units
∇	Vector differential operator	$[-]$
τ	Viscous stress term	$\left[kgm^{-1}s^{-2}\right]$
ε	Turbulent Eddy Dissipation Rate	$\left[m^2s^{-3}\right]$
ω	Specific Turbulence Dissipation Rate	$\left[s^{-1}\right]$

Symbol	Description	Units
ϕ	Equivalence Ratio	$[-]$
ψ	Fuel to Air Ratio	$[-]$
ρ	Density	$\left[Kgm^{-3}\right]$
μ_t	Eddy viscosity	$\left[kgm^{-1}s^{-1}\right]$
η	Efficiency	$[-]$

Subscripts and superscripts

Abbreviation	Meaning
st/stoich	Stoichiometric

Contents

1 Introduction

This chapter is comprised of a brief background on gas turbine engines (GTE), a short history of Siemens Energy as a manufacturer of gas turbine engines, literature study, problem formulation, objectives of this master thesis, and finally, the limitations of this study.

1.1 Background

The world has witnessed many innovations and breakthroughs throughout its history; however, none of these achievements could have been possible without the use of reliable energy sources. From the use of coal as an energy source in China in 2000 BC for cooking food to providing electricity for an entire city from nuclear power plants in the twenty-first century, humans have always found their way to exploit different sources, either renewable or nonrenewable. With the growing energy demand, sustainable development has forced countries to look for alternative methods of producing energy with less environmental impact. Hence, renewable energy sources such as solar, wind, hydro, geothermal, and biomass have gained immense popularity. Nonetheless, due to the intermittent nature of most of these renewable energy sources, some alternative methods should be considered to provide nonstop energy to different sectors.

Gas turbine engines are one of the most reliable alternatives to produce energy. Nevertheless, there are many other factors apart from reliability when it comes to utilizing gas turbine engines, including efficiency and emissions. In recent years, the focus has primarily been on reducing pollutants like Unburned Hydrocarbons (UHC), Carbon Monoxide (CO), and Nitrogen Oxides (NOx); however, the path to reducing emission is sometimes opposite to increasing the efficiency of the system. This is mostly dominant if the flame temperature is raised to increase efficiency, but with a higher working fluid temperature, NOx emissions can typically be raised. On the other hand, if temperature is reduced to decrease NOx, this typically results in higher CO and UHC levels due to incomplete combustion processes [1].

Nowadays, in most stationary gas turbine engines, NOx is the primary pollutant which is undesirable because it not only is an air pollutant by itself, but it also reacts in the atmosphere to form ground-level ozone (O3) and acid rain [2]. NOx is a term used for nitrogen oxides that include Nitrogen Monoxide (NO) and Nitrogen Dioxide (NO2), and there are three sources of NOx in gas turbine exhausts. The first source is called thermal NOx, and it is caused when nitrogen in the oxidizer, air, is combined with O and OH radicals, which are abundant in the flame. This process is known as the fixation of atmospheric nitrogen in the flame. Thermal NOx is exponentially related to temperature, which makes temperature the best mechanism to control thermal NOx emissions. The second source is fuel NOx, and it happens when nitrogen is chemically bonded to the fuel, almost all of it can convert into NOx. Most gaseous fuels do not contain fuel-bound nitrogen, while it is often found in liquid fuels. Untreated fuel oil can contain over 1000 ppm of fuel-bound nitrogen and this simply could lead to 40 ppm of NOx at the exhaust of the gas

turbine engine just from this mechanism [3]. The third source is called prompt NOx, and it is attributed to the reaction of combustion radicals with atmospheric nitrogen at the early stages of combustion. This mechanism cannot be quenched since the length scales are small and it becomes more prominent when other NOx formation mechanisms have been eliminated [3].

Throughout the years, a variety of different explanations have been proposed to describe the behavior of NOx pollution caused by gas turbine engines based on their design; nonetheless, it has been validated that the aggregate of all the above-mentioned NOx formation mechanisms has an exponential relationship to the combustion primary zone temperature. Therefore, reducing the flame temperature by different means can have a significant impact on NOx emissions. As will be discussed in detail in chapter 2.1, obtaining a well-premixed lean mixture of fuel and air is one of the most applicable and popular methods to reduce NOx emissions. A lean mixture provides a lower flame temperature and this leads to lower NOx emissions. Moreover, a well-premixed mixture of fuel and air eliminates local high fuel concentration in the mixture, and consequently, it eliminates local high temperatures [4, 5]. Nevertheless, the use of such a system can have its disadvantages if not designed properly such as decreasing the reliability and the range of stable operation [6].

With the growing interest in reducing carbon emissions in the world, many countries have shown interest in carbon-free fuels. Hydrogen is an attractive alternative to fossil fuels like natural gas because of its wide flammability range, large flame propagation speed, and small quenching distance. Hydrogen has a higher stoichiometric adiabatic flame temperature compared to methane, which causes more NOx emissions; however, this issue can be rectified with a leaner mixture of hydrogen and air, used for combustion. The main disadvantage in using most of the highly reactive fuels like hydrogen is that there is a high possibility of flashbacks due to their higher flame speed. Furthermore, a very lean mixture of hydrogen and air can lead to thermoacoustic instabilities [7].

Therefore, designing the combustor poses many challenges to the engineers as many geometric parameters can play crucial roles in the flow exiting the combustor of a gas turbine engine [8]. One of these geometric parameters is the location of the fuel nozzles, also known as fuel holes, in the burner, and finding their optimum location can not only reduce the NOx emissions significantly by providing a well-premixed mixture, but it also can eliminate the risk of flashbacks in the burner when a highly reactive fuel is used. Theoretically, there are three main methods to find the location of fuel holes namely, analytical, experimental, and numerical methods. Since gas turbine engines have very complex geometries and physics, it is practically impossible to address this problem analytically. By the same token, using experiments to try out different configurations of fuel holes can end up being a costly process. Therefore, Computational Fluid Dynamics (CFD) can be implemented as a powerful numerical tool to predict the premixed flow behavior, and based on that, necessary optimizations can be performed. However, there always are some questions aimed at the applicability of CFD, including how detailed should the physical model be, and how well does it represent real operating conditions? Since computational costs are directly related to the resolution of the numerical grid and models chosen for the analysis, how much computational resources are available? The choice of

turbulence modelling approach can also significantly affect the computational costs, and therefore, it is relevant to ask how detailed turbulence is needed to be solved. It is trivial that CFD has its limitations as a tool for predicting fluid flow, but the results obtained can be both verified and validated to ensure a realistic solution is obtained. In the end, this powerful tool can drastically reduce costs by eliminating unnecessary experiments for problems that do not have an analytical solution, if utilized properly.

1.2 Siemens Energy AB

Siemens AG is a German multinational conglomerate corporation that started from a small workshop in Berlin in October 1847 by Werner von Siemens and Johan Georg Halske. This company was initially called Telegraphenbauanstalt von Siemens & Halske, and it built the first long-distance telegraph line in Europe from Berlin to Frankfurt am Main in 1848 [9]. In 1866, one of the most important breakthroughs of Siemens happened when Werner von Siemens discovered the dynamo-electric principle based on Michael Faraday's work and produced a dynamo machine, a forerunner of modern generators.

The invention of the dynamo paved the way for other ways of transforming mechanical energy into electrical energy. In April 2020, Siemens Energy AG was formed by the spin off of the former gas and power division of the Siemens group [10]. Siemens Energy produces gas turbine engines with different power outputs from 2MW to 600 MW for a variety of different purposes.

Siemens Energy AB in Finspång, Sweden is one of the branches of Siemens Energy which has focused on producing gas turbine engines. This production site was initially a steam turbine factory named Svenska Turbinfabriks Aktiebolaget Ljungström (STAL), built by Birger och Fredrik Ljungström in 1913. Under the commission of the Swedish Air Force, this company started to develop three different jet engines and later applied the obtained knowledge to stationary gas turbine engines. STAL had undergone many structural and name changes until 2003 when Siemens purchased the company named Alstom Power Sweden AB at the time [11].

1.3 Problem Formulation

As one of the methods to reduce emissions, especially NOx, is to provide a lean premixed mixture of fuel and air to the combustor of a gas turbine engine, it is of prime importance to ensure high quality premixing occurs. This well-premixed mixture eliminates fuel concentrations in the burner and consequently, eliminates the local high temperatures leading to a reduction of NOx. The importance of premixing is exacerbated when highly reactive fuels like hydrogen are used in the burners, since the laminar flame speed, which is defined as the velocity at which the front of a premixed flame propagates relative to the unburned mixture [12], is higher than natural gas, and thus, there exists a high risk of flashbacks. Flashback is the uncontrolled and undesirable upstream flame propagation due to a local imbalance in the flow and flame velocity, causing damages to the burner [13]. In this case, it is desirable to reduce the fuel concentrations near the walls, where there are boundary layers with low velocities, such that the risk of flashbacks is removed.

Safari in his master thesis conducted at Siemens Energy AB tried to improve the location of fuel nozzles on the fuel pin located in main channels 1 and 2 of SGT-750, in order to have a flat fuel profile in the middle indicating a well-premixed mixture while decreasing the fuel concentrations near the walls to reduce the possibility of flashbacks [14]. Although his efforts provided a better understanding of the relation of fuel mixture in main channels 1 and 2, and the distribution of fuel nozzles on the fuel pin, it was later found that the results of chosen numerical schemes, turbulence models, and the optimizations performed, were not accurate. This was primarily due to the fact that the jets exiting the fuel nozzles were not captured completely, and therefore, some errors were involved in his simulations. Thus, Charoenchang in her master thesis conducted at Siemens Energy AB tried to improve the mesh used for the SGT-750 burner by using jet in the crossflow model and evaluating the mesh strategies tested at the combustion department at Siemens Energy AB [15]. She tried to reduce the number of cells, and at the same time keep the accuracy as high as possible, and in the end, she validated her data with the experimental results obtained for Jet in the Crossflow case. Furthermore, she aimed for finding a turbulence model which has acceptable computational costs while providing reasonable accuracy [15]. Her efforts resulted in a grid strategy that could be used for future works, such as to implement her findings for improving the geometry of the current SGT-750 model.

This master thesis tries to utilize an accurate grid and numerical models among the strategies tried so far for the SGT-750 burner based on Charoenchangs work [15] and improves the location of the fuel holes in main channels 1 and 2 based on Safaris work [14], in such a way that it reduces the NOx emissions by providing a well-mixed mixture of fuel and air, and low concentrations of fuel near the wall to reduce the risk of flashback in the burner for highly reactive fuels. In other words, this thesis initially aims at finding a reliable, grid-independent CFD methodology for studies and improvement of fuel hole placement, by combining the two previous master theses performed by Safari [14]and Charoenchang [15] for SGT-750 prototype burner. For CFD simulations in this thesis, Simcenter Star-CCM+ will be used, and for improvements, Design Manager will be implemented to sweep the location of fuel nozzles.

1.4 Objectives

As investigating gas turbine engines can be a vast topic involving many different specialties, it is crucial to limit the scope. Thus, this study tries to achieve several objectives in the following order:

- To evaluate the performance of three turbulence models namely, k-ε Realizable, k-ε Lag-EB, and k-ω SST.
- To evaluate how improvement techniques may be used to improve fuel-air mixing.
- To apply the above knowledge to the SGT-750 prototype burner while considering the maximal flashback resistance and low NOx emissions.
- To provide recommendations for future CFD optimization analysis.

1.5 Limitations

- To reduce the computational costs, several assumptions have been made including modeling a portion of the full model, section 3.1. Although these assumptions compromise the accuracy of the final results, they are carefully made by considering cost vs accuracy perspective.
- As it has been demonstrated in the results section, the turbulence models used for combustion simulation are steady RANS, which due to insufficient convergence, may result in frequent oscillation of the variables. The use of steady RANS is primarily due to the reduction of computational costs during the geometry improvements.
- For improvement of the location of the fuel holes, the variables should be limited to a reasonable number, otherwise, this can lead to many heavy simulations and therefore, it unnecessarily increases the computational time. On the other hand, if the number of variables is limited significantly, this can lead to an unsatisfactory and inaccurate optimization.
- As one of the most important steps in numerical simulation is validation of the data with either experimental or analytical data, this step cannot be performed within the time frame of this work.

1.6 Thesis Outline

This report first presents the theory behind the methodology and knowledge applied to this work in section 2; thereafter, provides the methodology in section 3, in which the assumptions and simplifications, geometry, mesh, solver setup, and boundary conditions are included. In the results section presented in section 4, the outcome of the evaluation of different turbulence models, as well as improvements on the location of fuel nozzles in main channels 1 and 2 are depicted, and it is followed by the discussion providing an explanation for the obtained results in section 5. In section 6, the conclusion summarizes this thesis work, and ultimately some recommendations for future work and the perspective of the study are presented in sections 7 and 8 respectively.

2 Theory

2.1 Gas Turbine Engines

Gas turbine engines are a form of the internal combustion engine (ICE) that run on an open cycle, and they consist of three main components namely compressor, combustion chamber or burner, and turbine, which converts the chemical energy of gaseous or liquid fuels into kinetic energy. Based on the function of gas turbine engines, other components might be added to the upstream or downstream of the engine, including propellers, nozzles or diffusers, etc. Gas turbine engines can be divided into two main categories of aero engines and stationary engines [16]. Aero gas turbine engines are primarily used for producing thrust force in airplanes, while stationary gas turbine engines are used for a variety of different purposes including generating electricity. These engines can have a power output of between a few Megawatts (MW) for small industrial gas turbine engines to the order of 500 MW for large gas turbine engines, with a range of 20 to 1000 kg/s of exhaust mass flow rate and a range of 10 to 25 for pressure ratio [17].

Ideal gas turbine engines operate on the Brayton cycle, and therefore, three processes are involved in these engines [18](figure 2).

1. Compression: For the gas turbine engine to produce useful work, the working fluid is compressed in the compressor. As it is evident from figure 2, both pressure and temperature are increased isentropically from state 1 to state 2.

2. Heat addition: Heat is added to the compressed working fluid in the burner by injecting fuels and burning the mixture. This process is assumed to be isobaric, as heat is added to the working fluid from state 2 to state 3 in figure 2. Without this stage, in the most ideal system where there are no losses, all the work transferred to the compressor is equally extracted in the turbine.

3. Expansion: Working fluid undergoes an isentropic expansion process in the turbine that is caused by the reduction in pressure. At this stage, the required work based on the application of a gas turbine engine is extracted from the working fluid. This process is from state 3 to state 4 in figure 2.

As the name implies, there are some assumptions and simplifications included in ideal gas turbine engines, including the isentropic compression and expansion and constant pressure heat addition; however, in reality, the efficiency of the engines can be significantly lower due to losses not taken into account in the ideal assumptions. As table 5 indicates, the actual efficiency is lower than the ideal efficiency for different engines.

In a major category, gas turbine engines can be classified based on the air path and how power is produced. Figure 3 demonstrates different types of gas turbine engines. Nowadays, most stationary gas turbine engines are turbofan, which implies that a portion of the air passes through the bypass around the combustion chamber, and another portion of air is used for combustion and cooling inside the burner. The advantage of turbofan engines is that they are extremely fuel-efficient such that

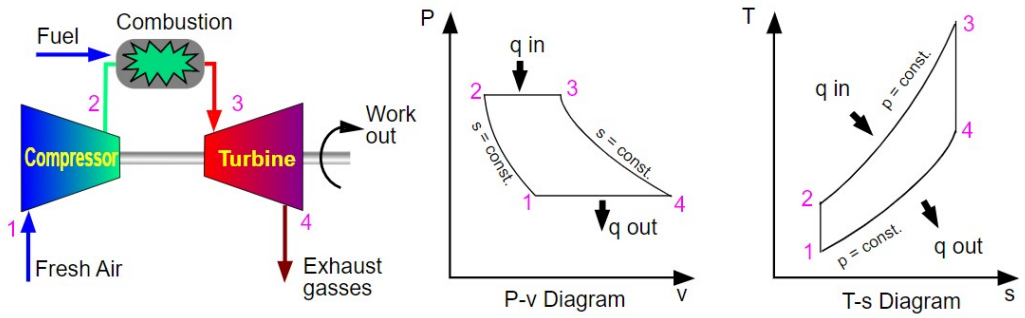

Figure 2: Ideal gas turbine engine cycle and its P-v and T-S diagrams [19] License Creative Commons (CC BY-SA 3.0)

.

Table 5: The ideal and actual efficiency of different gas turbine engines [20]

	Saturn 20	**Centaur 40**	**Taurus 60**	**Titan 130**	**Titan 250**
$\eta_{Ideal}[\%]$	41	48	51	56	60
$\eta_{Actual}[\%]$	24.5	28	32	36	40

even low bypass ratio turbofan engines are more efficient than turbojet engines.

2.1.1 Combustion Chamber

Since gas turbine engines are immensely utilized in the industry, the pollution caused by these engines is also of prime importance. Hence, the combustion chambers in gas turbine engines have probably undergone the most change, since they are directly related to the efficiency of the system as well as the amount of pollution produced by the system. Combustion chamber, also known as burners or combustors, is where heat is added to the working fluid by injecting fuel and burning the mixture. The components in the burners highly depend on the application of the burners; however, some parts such as diffuser, liner, casing, and cooling arrangement exist in most of the combustors [22].

Conventional burners generally have three zones known as the primary zone, secondary or intermediate zone, and tertiary or dilution zone. The primary zone is where most of the fuel is injected into the chamber and combustion takes place. In the secondary zone, another portion of the air is mixed with the burnt mixture through secondary holes so that fuel molecules like CO and radical H can be fully oxidized [23]. Since the air leaving the secondary zone has a temperature beyond the tolerance of the turbine blades, the last portion of the unburned air is injected into the chamber to cool down the fluid in a zone known as the dilution zone.

In a major classification, the burners of gas turbine engines can be divided into three groups based on their configurations. They are Can type, Annular type, and Can-annular type.

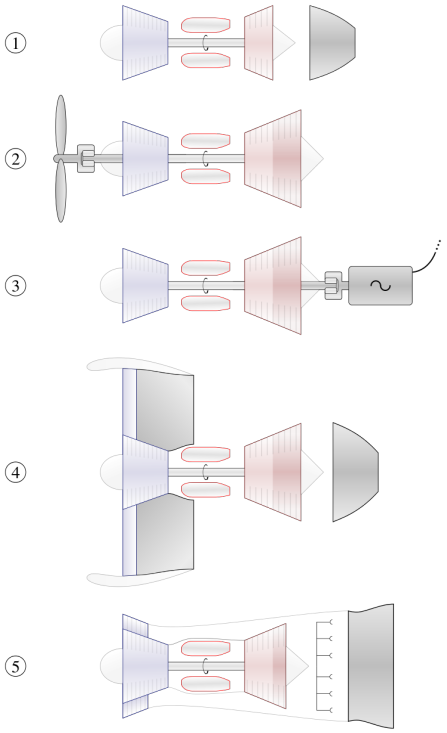

Figure 3: Different types of gas turbine engines: 1. Turbojet, 2. Turboprop, 3. Turboshaft with Electric Generator, 4. High Bypass Turbofan, 5. Low Bypass Afterburning Turbofan [21] License Creative Commons (CC BY-SA 3.0)

.

Can Type

This burner is sometimes referred to as a multiple or tubular burner and it consists of several cylindrical chambers located around the shaft which connects the turbine to the compressor, figure 4. The compressed air delivered from the compressor is divided into multiple streams, and each would supply a chamber. Since the air leaving the diffuser vanes is already divided into equal portions, these burners are best suited for axial-flow engines especially when centrifugal compressors are used. Moreover, for better pressure fluctuation stabilization, the chambers are connected. Although these burners are mechanically robust, they have high-pressure losses, and they are bulky and heavy, which makes them hard to utilize in the aerospace industry. [18].

Annular Type

In this type, an annular liner is located concentrically in an annular air casing. As it is clear from figure 5, this configuration provides an aerodynamically 'clean' and robust layout which results in a compact design, and consequently, less pressure drop and less surface area compared to other configurations. These engines are best used when there is an axial-flow compressor, and as of today, most of the aero-engines use this configuration [18].

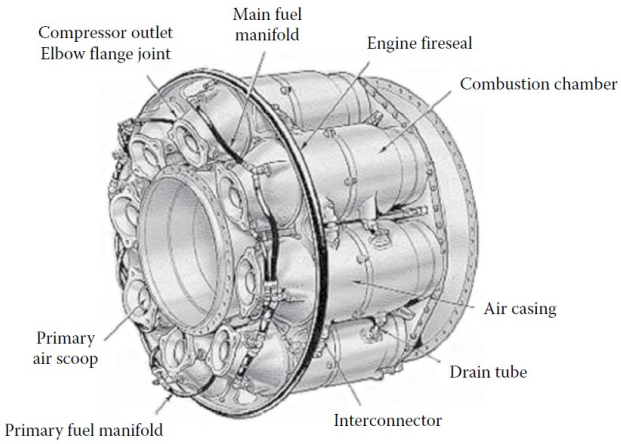

Figure 4: Can type burner [24] ©Rolls-Royce plc (1996). Reprinted with permission from the copyright holder.

Can-annular Type

This configuration is also known as tubo-annular or cannular and is a combination of annular and can-type burners. In this layout, the cylindrical chambers are located in a single annulus as shown in figure 6. This design has the best features of the two previously mentioned types including having low-pressure losses and being mechanically robust; nevertheless, there come some disadvantages with this design as well like it requires connectors.

2.1.2 Modes of Combustion

As the gas turbine technology has progressed over the years, huge efforts have been invested in discovering methods to increase the efficiency of the burners and decrease their emission at the same time. These efforts have led to creation of multiple different combustion processes known as Non-premixed Flames and Premixed Flames.

Non-premixed Flames

The most traditional and common type of combustion is conventional or Non-premixed combustion where fuel and oxidizer are introduced separately to the chamber. These flames are characterized by their high stability and high local firing temperature, and they can be controlled by the rate at which oxidizer and fuel are transported. Candles are one of the most basic examples of conventional flames. This flame is also referred to as diffusion flame since diffusion dominates the supply rate in laminar non-premixed flames, while, for turbulent non-premixed flames, both diffusion and turbulent mixing, control the supply rate. Once the fuel and oxidizer are mixed, they burn near the stoichiometric conditions where all of the fuel and oxidizer are consumed. One of the drawbacks of this flame is its high NOx emissions due to its high local firing temperature [17]. Thus, to reduce NOx emissions, the temperature of the flame could be reduced by a method called Wet Low Emission (WLE). This method primarily focuses on injecting steam or water into the primary

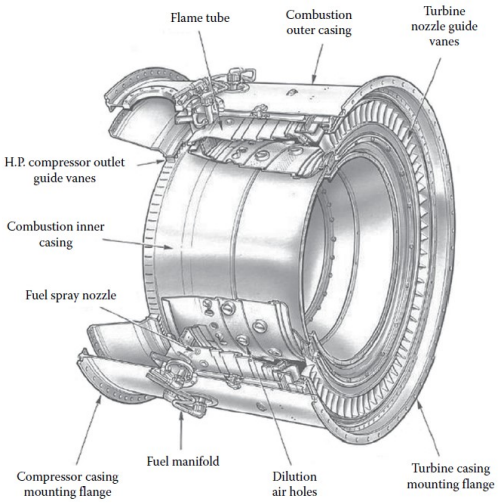

Figure 5: Annular type burner [24] ©Rolls-Royce plc (1996). Reprinted with permission from the copyright holder.

zone in the combustion chamber to reduce the flame temperature and consequently, reduce NOx [25]. The downside of this method is that it requires a network for transferring purified water or steam as well as fuel which makes the maintenance harder and more expensive. Furthermore, this method can lead to an increase in CO emissions and as explained in the next paragraph, it does not significantly reduce NOx emissions compared to Dry Low Emission (DLE) [26].

Premixed and Partially Premixed Flames

Contrary to Non-premixed flames are premixed flames. In these flames, fuel and oxidizer are mixed before entering the primary zone of the combustion chamber. The major advantage of these flames is that to reduce the NOx emissions, there is no need to include a network of water or steam to reduce the flame temperature. Instead, in this method, if the amount of oxidizer is more than the amount of fuel, a lean mixture of fuel and air, all of the fuel is consumed with a portion of the oxidizer, and the remaining oxidizer is used to cool down the flame [27].

This method, lean premixed flame (LPM), is one of the methods known as Dry Low Emission (DLE) to reduce NOx emission in premixed flames. The main difference between premixed and non-premixed flames is that, in non-premixed burners, on one side of the flame there are combustion products and on the other side of the flame, there are separate streams of fuel and oxidizer which do not burn on their own; however, in premixed flames on one side there are combustion products and on the other side, there is a mixture of fuel and air which is highly flammable and if not designed properly, flashbacks can occur into the burner leading to a shorter lifetime of components in the burner [17]. This is one of the disadvantages of the premixed flames, and for rectifying this problem, the mean flow velocity should be higher than the velocity of the planar flame of the gaseous mixture. Even under these considerations, there still is a risk of flashback in the regions where the mean flow velocity is low such as boundary layers [28]. Since there is excess air in the premixed mixture, another challenge in the premixed flame design arises. This challenge is the stability

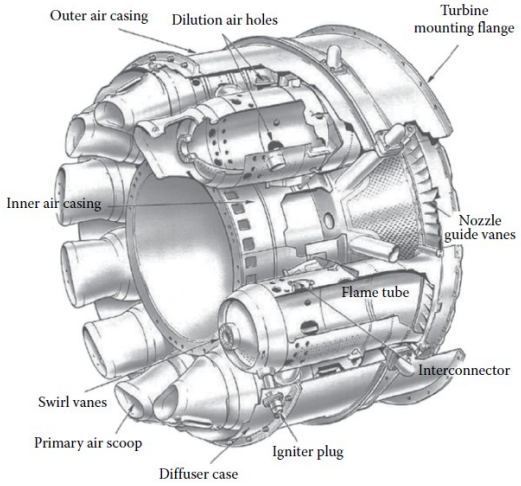

Figure 6: Can-Annular type burner [24] ©Rolls-Royce plc (1996). Reprinted with permission from the copyright holder.

of the flame, and it stabilizes where the local flow velocity matches the flame speed.

The use of different flames varies with their applications such that in aero-engines, for safety purposes, non-premixed burners are preferred; however, it is found that premixed burners, in general, can substantially reduce emissions, specifically NOx [4, 5]. Therefore, these flames are more favorable in stationary gas turbine engines.

In terms of differences in burner design for these two flames, lean premix burners should have a larger volume to ensure complete combustion at lower temperatures; moreover, these burners also have larger fuel injectors to provide a well-mixed mixture of fuel and air, to eliminate the local high-temperature regions, compared to conventional burners [3]. Although it is ideal to obtain a fully mixed mixture of fuel and air before combustion in premixed flame, it is highly unlikely to have such a mixture, and most of the time a partially premixed mixture is obtained [17].

As it is evident, the DLE method is more effective when it comes to reducing NOx. Therefore, these engines are hugely favorable compared to WLE, if the disadvantages including combustion dynamics and flame stability are carefully considered, forcing many companies and industries to utilize DLE for their applications. Siemens Energy AB is one of the companies that produce DLE gas turbine engines.

The Siemens SGT-750 and 4th Generation DLE Burner

SGT-750 is a lightweight industrial gas turbine engine with a gross power output of 39.8 MW (figure 7) [29]. With the new design of its 4th generation DLE burner, it guarantees to keep NOx emissions below 9 ppm. The SGT-750 has a 13-stage axial air compressor with two variable guide vanes ensuring reliable performance even in the most extreme conditions. Its can-type combustion system is serially cooled down and it consists of 8 cans and 8 transition ducts, suitable for both liquid and gaseous fuels. There are four separate controlled fuel lines in this burner namely Pilot Burner, Rich-Pilot-Lean (RPL) Burner which is intended for stabilization, and two channels named Main Channel 1 and Main Channel 2 [11]. The 4th generation

DLE burner can operate running on 40% hydrogen, and the air and fuel mixture has been improved with the help of swirler wings and quarls to provide a better premixed mixture to the combustion chamber and stabilize the flame, figure 8. This engine has a 2-stage power turbine which can be optimized for ambient conditions, from cold to hot climates [30].

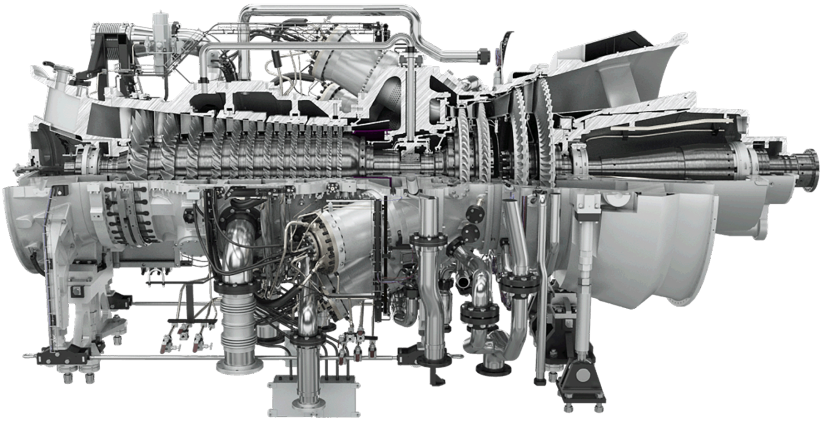

Figure 7: SGT-750 gas turbine engine manufactured at Siemens Energy AB [30] ©Siemens Energy AB (2022). Reprinted with permission from the copyright holder.

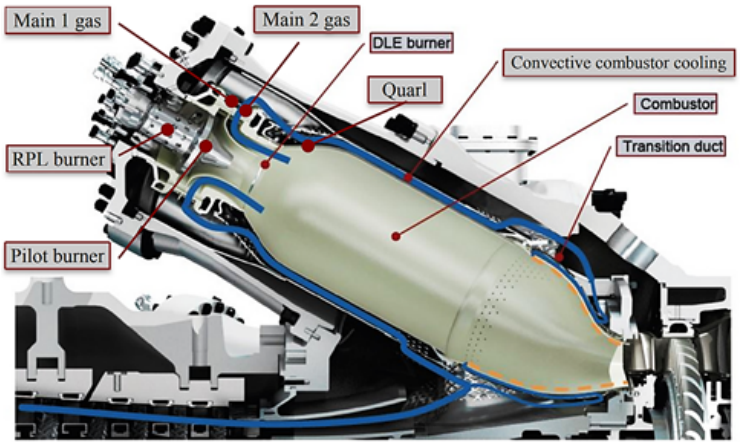

Figure 8: The combustion chamber in SGT-750 [31] ©Siemens Energy AB (2022). Reprinted with permission from the copyright holder.

2.2 Computational Fluid Dynamics (CFD)

Predicting the behavior of the fluid by the means of analytical, experimental, or computational methods is of prime importance in many engineering applications. The analytical or theoretical method, which is the most accurate of all, is when the equations describing a physical phenomenon are solved with the help of classical

mathematics. Despite the immense contributions of this method, in most engineering cases, utilizing this method requires many assumptions and simplifications of the complicated governing differential equations, which as a result provides unrealistic results. As an alternative, the experimental method is used, since it provides the most reliable information when the full-scale model is used for measurements. However, in most engineering applications, using the full-scale model is either impractical or difficult and expensive. Thus, sometimes a small-scale model is used for experiments, and the data are extrapolated for the full-scale model. In order to reduce the costs of experiments and remove the problems involved in the analytical method, Computational Fluid Dynamics or CFD is used [32].

Perhaps the first major example of using CFD is the work of Kopal in preparing tables of supersonic flow over sharp cones by numerically solving the differential equations [33]. CFD is the knowledge of analyzing systems involving fluid flow, heat transfer, etc by means of computer-based simulations. CFD is such a powerful tool that is used frequently in aerospace and mechanical industries, heating, ventilation, and air conditioning (HVAC) of buildings, and the energy sector. In the gas turbine industry, CFD is applied in different parts such as compressor and turbine sections to analyze the fluid flow around the blades in turbomachines, or in the combustion chamber to predict the flow before and after the combustion [34]. Despite the ease of using CFD as a tool for problems in fluid mechanics, it is worth mentioning that this method has some limitations such as possible uncertainties, or errors involved in numerical methods. Numerical algorithms constitute the core of CFD, and there are many companies that offer CFD packages for greater ease for the users. Most of these packages contain three elements (1) Pre-processor,(2) Processor or solver, and (3) Post-processor.

Pre-processing

In pre-processing, the geometry of the problem known as the computational domain is defined. This geometry is later divided into a grid of many smaller cells which is called mesh. The accuracy of the CFD model is dependent on the resolution of the grid to a huge extent, and usually, the finer the mesh, the more accurate the solution is, since the solution to a flow problem is defined at nodes inside each cell. However, as the grid becomes finer, the computational expenses such as the time to solve the problem increases, therefore, a reasonable balance between the accuracy and the computational expenses should be found. Thereafter, the right physical models, boundary conditions, initial conditions, convergence criteria, and fluid and solid properties are applied to ensure the computational model is a correct simulation of a physical model [34].

Processing

There exist three main numerical solution techniques for solving fluid problems computationally. They are Finite Difference Method (FDM), Finite Element Method (FEM), and Spectral Method. There is a special formulation of FDM called Finite Volume Method (FVM) that rectifies the deficiencies of the FDM and is used in many CFD solvers including ANSYS CFX, ANSYS FLUENT, and STAR-CCM+. In FVM, the governing equations of the fluid flow are integrated over all the control

volumes of the domain. Then, the differential equations are discretized to obtain a system of algebraic equations. Since the underlying physical phenomena are complex and non-linear, an iterative method is required to find the solution. [34]

Post-processing

When the solution is converged, it is practical to post-process the obtained data with the help of available tools such as geometry and grid display, vector plots, line and shaded contour plots, and 2D and 3D surface plots. Post-processing can give meaning to the data and significantly ease the understanding of the fluid flow behavior. [34]

2.2.1 Governing Equations

The governing equations in fluid mechanics describe the conservation laws of physics, namely, the conservation of mass, momentum, and energy. These governing partial differential equations can be solved numerically together with other equations for different physics such as the equation of state for a compressible fluid. From here on, bold letters and signs represent vectors and their corresponding operations while, regular letters demonstrate scalars.

Conservation of Mass

Conservation of mass states that the rate of increase of mass in a fluid element is equal to the net rate of flow of mass into the fluid element, and its governing equation can be written as [34]:

$$\frac{\partial \rho}{\partial t} + \nabla \cdot (\rho \mathbf{U}) = 0 \tag{1}$$

where ρ, t, and $\mathbf{U}$ are density, time, and velocity vector in three dimensions respectively. This equation is an unsteady, three-dimensional continuity equation at a point in a compressible fluid where the first term in equation 1 shows the density change with time that accounts for compressibility effects in an infinitesimally small control volume, and the second term is mass flux rate through the surface of the control volume, and this is done by measuring the divergence of a vector field $\nabla \cdot \mathbf{U}$, which in this case is the velocity vector.

Conservation of Momentum

Conservation of momentum is obtained from the second law of Newton which mentions the rate of change of momentum of a fluid element is equal to the sum of the forces on the element.

$$\frac{\partial (\rho \mathbf{U})}{\partial t} + \nabla \cdot (\rho \mathbf{U}\mathbf{U}) = \nabla \cdot P + \nabla \cdot \tau + F_b \tag{2}$$

where τ and P are the viscous stress and pressure term respectively, and F_b indicates the body forces [34].

Conservation of Energy

The energy equation is obtained from the first law of thermodynamics and it states that the rate of change of energy of a fluid particle is equal to the rate of heat addition and work done on the particle. The governing equation for the conservation of energy can be written as:

$$\frac{\partial(\rho E)}{\partial t} + \nabla\cdot(\rho E\mathbf{U}) = \nabla\cdot(\mathbf{U}\sigma) + F_b.\mathbf{U} - \nabla\cdot q + S_E \tag{3}$$

where E is the total energy per unit volume, q is heat flux, and S_E is the energy source per unit volume [34].

Equations of State

In problems involving compressible fluid, the system of equations comprising of equations 1, 2, and 3 are not sufficient, since they contain seven unknowns, ρ, P, T, and E, as well as u, v, and w which are the velocity components of the velocity vector, while there only exist five equations. Therefore, additional equations must be added to close the system of equations. One of these equations is the equation of state for ideal gases which assumes that their intermolecular forces are negligible, and it relates the pressure to the state variables. The ideal gas equation of state is as follows:

$$P = \rho RT \tag{4}$$

where R is the specific gas constant. As for E, since the total energy of a fluid is the sum of the internal, kinetic $\frac{1}{2}(u^2 + v^2 + w^2)$, and gravitational potential energies, only the internal energy requires an additional equation which can be addressed by the following relation:

$$i = C_v T \tag{5}$$

where i is the internal energy, and C_v is the specific heat at constant volume [34].

2.2.2 Turbulence

Turbulence is a physical phenomenon that happens frequently in nature, from internal flows in a straight pipe to the flow around the wings of an airplane. Turbulence is involved in many engineering applications such that understanding its behavior is of prime importance for many design criteria. Although there is no clear definition for turbulence, it is most often quantified with Reynolds Number which is defined as the ratio of inertial forces to viscous forces, and its value, based on the geometry, flow characteristic, and the fluid, determines if the flow is either laminar or turbulent. When talking about turbulence, a number of characteristic features such as irregularity and chaotic fluctuations in space and time, diffusivity, dissipation of kinetic energy for eddies, and happening in three dimensions and at large Reynolds Numbers are noticed [35]. There exist different methods to predict turbulence such as Direct Numerical Simulation (DNS), Large Eddy Simulation (LES), Steady Reynolds Average Navier-Stokes (RANS), or Unsteady Reynolds Average Navier-Stokes (URANS) models. Among these models, DNS is the most accurate

of all, however, that comes at the cost of heavy computational costs due to not using any turbulence modeling and direct discretization of the governing equations, which generates large quantities of data. On the other hand, RANS models possess an acceptable accuracy in certain problems, but they are the least computationally expensive. RANS turbulence models calculate the time-averaged variables by the Reynolds decomposition method. This method decomposes the instantaneous properties into a time-averaged or mean, and a fluctuating variable in the following form:

$$\phi = \overline{\phi} + \phi' \tag{6}$$

where $\overline{\phi}$ and ϕ' are respectively mean and fluctuating components of the instantaneous variable ϕ. By applying this method on all the existing variables in equations 1, 2, and 3, they can be rewritten in the following form:

$$\frac{\partial \rho}{\partial t} + \nabla\cdot(\rho\bar{\mathbf{U}}) = 0 \tag{7}$$

$$\frac{\partial(\rho\bar{\mathbf{U}})}{\partial t} + \nabla\cdot(\rho\bar{\mathbf{U}}\bar{\mathbf{U}}) = -\nabla\cdot\bar{P}I + \nabla\cdot(\bar{\mathbf{T}} + \mathbf{T_{RANS}}) + F_b \tag{8}$$

$$\frac{\partial(\rho\bar{E})}{\partial t} + \nabla\cdot(\rho\bar{E}\bar{\mathbf{U}}) = -\nabla\cdot\bar{P}\bar{\mathbf{U}} + \nabla\cdot(\bar{\mathbf{T}} + \mathbf{T_{RANS}})\bar{\mathbf{U}} - \nabla\cdot\bar{\mathbf{q}} + \mathbf{F_b}\cdot\mathbf{U} \tag{9}$$

where $\bar{P}$, and I, are pressure tensor, and identity matrix respectively. As it is clear from the above equations, the stress tensor, is divided into viscous stress tensor ($\bar{T}$), and average Reynolds stress tensor (T_{RANS}), which the latter must be modeled without adding more unknowns than the available equations. This is often referred to as the closure problem within turbulence modeling.

One way to address this problem is by assuming that the Reynolds stress tensor is related to the strain rate tensor and turbulent viscosity. This is done by Boussinesq assumption in the following form:

$$\mathbf{T_{RANS}} = 2\mu_t\mathbf{S} - \frac{2}{3}(\mu_t\nabla\cdot\mathbf{U} + \rho k)\cdot\mathbf{I} \tag{10}$$

where $\mathbf{S}$ is the strain rate tensor, and k is the turbulent kinetic energy. In Reynolds Average Simulation (RAS), the eddy viscosity is often modeled by using two equation models where one transport equation is solved for the kinetic energy and one equation is solved for the turbulent eddy dissipation rate [17]. Two of the most famous models categorized in this group are k-ε and k-ω.

$k-\varepsilon$ Turbulence Model

The standard $k-\varepsilon$ turbulence model is one of the most recognized turbulence models that have been revised continuously for decades and have been proven to provide reasonable accuracy in dealing with turbulence. This model solves for both Turbulent Kinetic Energy (TKE), denoted with k, and turbulent eddy dissipation rate, denoted with ε, by using two transport equations. These parameters are later used to find the eddy viscosity by using the following equation:

$$\mu_t = \rho C_\mu \frac{k^2}{\varepsilon} \tag{11}$$

where C_μ is turbulent viscosity and it is constant. However, in this model, at high strain rates, the interactions within the fluctuating velocity components can appear negative. To solve this problem, the realizable model of $k-\varepsilon$ is introduced, which assumes that the turbulent viscosity is variable by using a new formulation, and uses a new transport equation for the turbulent eddy dissipation rate [35, 36].

Another variety of the standard $k-\varepsilon$ model is the Lag Elliptic Blending (Lag EB) model. Lag EB is an ε-based model that was developed by Lardeau and Billard [37], and it solves for turbulent eddy viscosity by solving for turbulent kinetic energy, turbulent dissipation rate, and adding a factor of elliptic blending to improve low Reynolds near-wall solution and to avoid over-prediction of turbulent kinetic energy. Furthermore, the standard $k-\varepsilon$ model assumes the stress and strain tensors to be aligned. Since in reality, it is not always the case, Lag EB model considers the possibility of the misalignment between these two tensors. This model is known to have the best of both Realizable $k-\varepsilon$ and SST $k-\omega$ in dealing with fluid flow, as it has more stability compared to SST $k-\omega$ in complex geometries, and can predict near-wall regions better than Realizable $k-\varepsilon$.

$k-\omega$ Turbulence Model

The standard $k-\omega$ is a low Reynolds two-equation model where apart from the conservation equations, two transport equations are solved for the turbulent kinetic energy, which accounts for the energy in turbulence, and specific turbulent dissipation rate ω, which accounts for the rate of dissipation per unit turbulent kinetic energy. This is done to avoid the problem of modeling ε in near the wall region. This leads to the strength of $k-\omega$ compared to other RANS models, which is in resolving boundary layer problems subjected to adverse pressure gradients. Shear Stress Transport (SST) $k-\omega$ turbulence model is a combination of $k-\omega$ and $k-\varepsilon$ models which makes it suitable to use throughout the boundary layer as well as the free stream. SST $k-\omega$ also rectifies one of the drawbacks of $k-\omega$ models which is their sensitivity to ω value in inlet boundary conditions in internal flows [38].

2.2.3 Turbulence Wall Treatment

Since 1904 when Ludwig Prandtl came up with the physical description of the boundary layer, there have been many developments in this field such as finding new analytical relations, or mathematical models being implemented in the computational models [39]. Since boundary layers are a source of turbulence, it is of prime importance to capture them in CFD simulations properly. One way to do so is by generating a very fine mesh near the wall to capture the steep velocity gradients and other flow field parameters. However, this method drastically increases computational costs. Thankfully, an alternative exists for near-wall calculations with thicker mesh, without compromising much accuracy, which is known as the wall functions.

The wall boundary layer is categorized into three sub-layers based on y^+ and u^+ which are two dimensionless parameters and are defined as follows:

$$y^+ = \frac{y\rho u^*}{\mu} \tag{12}$$

$$u^+ = \frac{u}{u^*} \tag{13}$$

where u^* is described according to the type of the wall function. The use of these dimensionless parameters help to put all profiles on the same curve regardless of the type of fluid or velocity. The mentioned sub-layers in the boundary layer are, viscous sub-layer ($y^+ < 5$) where it is in direct contact with the wall and is dominated by viscous effects, Buffer sub-layer ($5 < y^+ < 30$), and Log-law sub-layer ($30 < y^+$) where turbulence is dominant.

2.3 Reacting Flow

For combustion modeling, it is convenient to assume that the components of a mixture are miscible in one phase for all flow modeling purposes. A multi-component or multi-species mixture assumes that the components of a mixture are miscible in one phase on a microscopic scale, and it is represented by a bulk density, etc. Thereafter, the species model considers the transport of species within this phase, where it is assumed that the species are completely miscible. Since different species have different material properties, mass fraction of different mixture components are calculated.

Multi-component mixture is either reacting or non-reacting in CFD simulations. Reacting flows are types of fluid flows involving chemical reactions happening between the interphase of different fluids or within the fluids. One of the most famous examples of reacting flow is combustion, which takes place in gas turbine engines or in general, internal combustion engines. There exist two methods to simulate reacting flows called Flamelet model, and Reacting Species Transport (RST) model, which the latter solves a transport equation for all the species in a mechanism, and later the obtained mass fractions are used to generate the products. This is done by calculating all reactions in each cell at each time step and iteration. This model is most suitable for cases where the mixing time scale is shorter than the reaction time scale, for example, transient combustion such as explosions, ignition, part-load conditions in combustors, etc [40].

On the other hand, in Flamelet model, the framework is set on the discretization of a large-scale turbulent flame into several one-dimensional flamelets; thereafter, instead of solving the conservation equations for all the species, they are solved for a set of flamelet variables that describe the thermochemical state in each CFD cell. This simplification drastically reduces the computational costs and making it more suitable for applications in full-load conditions in combustors, where the reaction time scale is shorter than the mixing time scale. In order to determine the combustion chemistry in flamelet model, a parameter is defined known as the Mixture fraction Z, which is described in detail in section 2.4 [40].

Each of these two models has different sub-models that can be implemented based on the purpose of the simulation; however, the sub-model of interest for this simulation, in the Flamelet model, is called Flamelet Generated Manifold (FGM). This model is based on the assumptions of the Flamelet model with some differences in the governing equations, which is suitable for premixed and partially premixed flames. Through this sub-model, combustion takes place in a thin layer that divides the domain into unburned to fully burned mixtures. Therefore, a variable is defined

known as progress variable c, which is used for tracking the combustion process in each cell. Value of $c = 0$ refers to no combustion, and value of $c = 1$ refers to complete combustion. Another benefit of this model is that flame ignition can be applied by the user at the desired iteration and position [40].

2.4 Equivalence Ratio

Fuel-to-air ratio can be expressed on a mass or volume basis. Stoichiometric fuel-to-air ratio is referred to when the combustion takes place with exactly the right amount of air to burn all the fuel. When more air is mixed with fuel than the stoichiometric fuel-to-air ratio, it is said that the combustion is fuel-lean, and on the contrary, when less air is mixed with the fuel, it is called fuel-rich. It is very convenient to normalize the fuel-to-air ratio for each fuel by the stoichiometric fuel-to-air ratio, and therefore, it is called the equivalence ratio (ER).

$$\phi = \frac{\psi_{actual}}{\psi_{stoich}} \tag{14}$$

where ϕ, ψ_{actual}, and ψ_{stoich} are equivalence ratio, actual fuel-to-air ratio, and stoichiometric fuel-to-air ratio. With regards to the equivalence ratio, the combustion is referred to as lean for $\phi < 1$ and rich for $\phi > 1$. In theory, the highest flame temperature, which is determined by a balance of energy between reactants and products, happens at $\phi = 1$. This is due to the fact that all the fuel and oxidizers are used in the process; however, in practice, the peak temperature is slightly above stoichiometric ($\phi \approx 1.05$). The flame temperature highly depends on the type of fuel such that the adiabatic flame temperature for Methane is 2223 Kelvin and for Hydrogen is 2370 Kelvin [1].

Equivalence ratio can also be defined based on mixture fraction, Z, which is the elemental composition that originated from the fuel stream, and it has a value between 0 and 1. Value of 0 means pure oxidizer, and a value of 1 means pure fuel. The relation between equivalence ratio and mixture fraction is as follows, where Z_{st} is the stoichiometric mixture fraction:

$$\phi = \frac{Z}{1 - Z} \frac{1 - Z_{st}}{Z_{st}} \tag{15}$$

3 Method

3.1 Assumptions and Simplifications

In most CFD simulations, it is beneficial if some simplifications and assumptions are made to reduce the computational costs without compromising the accuracy significantly. In this model, it is believed that the following assumptions can reduce computational costs while providing a reasonable accuracy to the solution.

- The simulations in this project are conducted on a thirty-degree slice of the full model with nominal geometry, no tolerances, and periodic boundary conditions applied on both sides of the model to reduce the total number of cells.
- Although this variant of SGT-750 used for this study utilizes different components, some of which are not included in the model to significantly reduce the number of cells. However, it is believed that the results are not affected by this simplification.
- Even though a portion of the fuel and air mixture goes through the Pilot and RPL for stabilizing the flame, they are not included in the model; however, velocity and temperature profiles from the full model are applied as a boundary condition to the geometry.
- For further simplification of the geometry, and since most of the focus in this study is on the premixing in the main channels, film cooling is not considered.
- In order to simplify the improvement of fuel-nozzles locations and to limit the variables used effecting this process, it is assumed that the fuel nozzles can only move along the burner axis, and their diameter is constant throughout the improvement.
- It is assumed that the walls in the combustion chamber are adiabatic which means there is no heat transfer through the walls of the combustion chamber.
- The leakages between the burner and the can, and between can and the T-duct are assumed to be negligible.
- Air which is the oxidizer in this simulation is assumed to be an ideal gas and is only composed of Oxygen (O) and Nitrogen (N), while the fuel is assumed to be only Methane (CH4).
- Compressibility effects in the combustion chamber are assumed to be negligible and therefore, a pressure-based solver is used for the simulations.
- Simulations conducted in this study are all done under steady-state conditions, which take a time average of the fluctuating components such as velocity and pressure, leading to less heavy simulations.

3.2 Geometry

The first step in any CFD simulation is the use of proper geometry. Figure 9 is a schematic section of one of the eight burners and combustion chambers in the SGT-750 combustion system. As it is clear, the burner has 4 separate fuel lines known as Pilot, RPL, Main 1, and Main 2. The fuel and air are mixed in this burner before they enter the primary zone of the combustion chamber. Before the mixture leaves the chamber to enter the turbine, it goes through a transition duct.

Since most of the fuel and air mixture enters the chamber from the main channels 1 and 2, it is of prime importance to ensure a homogeneous mixture is obtained. Therefore, right below every two fuel pins, there exists a swirler wing to create a recirculation zone to define the flame location. This would ultimately lead to better mixing of the mixture as well. For premixed systems, the upstream velocity must be higher than the turbulent flame speed to avoid flashback. Without a recirculation zone, the flame speed must be higher than the can velocity to avoid blow-off. Thus, by adding a recirculation zone, the risk of blow-off due to velocity imbalance is eliminated. Therefore, all premixed systems have a recirculation zone to define the flame location which also stabilizes the flame, figure 10. In each burner of SGT-750, there are 24 fuel pins and 12 swirler wings. Since the main objective of this thesis is to improve the location of fuel nozzles on the fuel pins, as well as keep the computational costs to a reasonable level, only a thirty-degree sector of the model that includes one swirler wing with two fuel pins on both sides is investigated. Furthermore, for simplicity in the calculations, and since the focus is mainly on main channels 1 and 2, the RPL and pilot burners are not included in the simulations and the velocity and temperature profiles from previous simulations of the full model are imported as a boundary condition to this model.

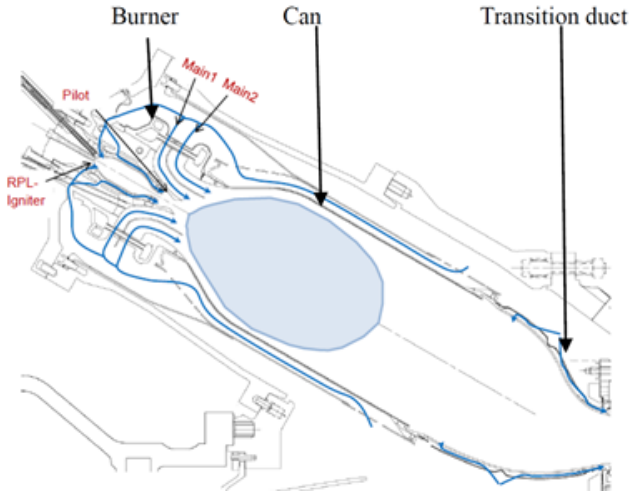

Figure 9: Mid-plane section of the full model ©O. Lindman (2014). Reprinted with permission from the copyright holder. [41]

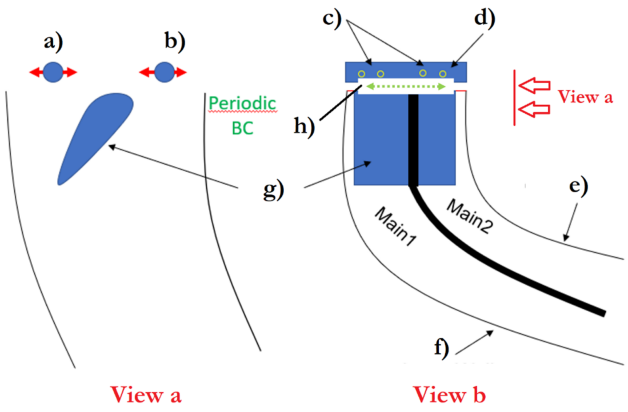

Figure 10: Schematic 30-degree section of the model including two fuel pins in two views a and b, a) left pin, b) right pin, c) fuel holes, d) fuel pin, e) outer wall (main channel 2), f) inner wall (main channel 1), g) guide vane and h) Fuel holes displacement [14] ©M. Safari (2020). Reprinted with permission from the copyright holder.

3.3 Mesh

As one of the most important steps in CFD simulations is to mesh the geometry, an appropriate strategy must be chosen in the domain. Charoenchang in her study investigated four different mesh strategies on a jet in crossflow and validated her results with experimental data [15]. Since the fuel that exits the fuel nozzles mixing with the oxidizer is similar to the jet in crossflow, it has been decided to implement the strategy that Charoenchang used in her master thesis. This includes inserting a cylindrical block with local refinement in the direction of the jet and another larger cylindrical block perpendicular to the direction of the fuel exiting the fuel hole, figure 11. It is extremely important to move the cylindrical blocks used for volumetric mesh refinement with the fuel holes, as they will move during the design improvement iterations.

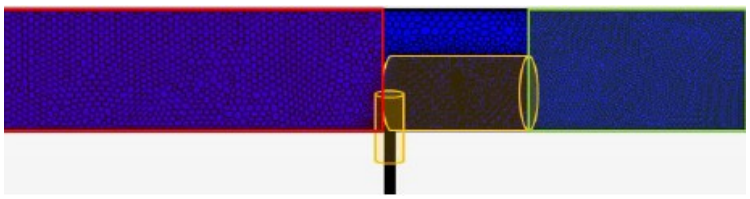

Figure 11: Grid strategy taken from Charoenchang master thesis [15] ©W. Charoenchang (2021). Reprinted with permission from the copyright holder.

Figure 12 demonstrates mesh resolution on the mid-plane in the geometry at different locations. As it is clear, finer mesh resolution has been applied to the regions where higher gradients may occur, or are of prime importance including near the wall regions and the exit of fuel holes. As it is clear from figure 12, much finer mesh at the outlet of fuel holes exist due to the use of cylindrical blocks used for volumetric mesh refinement. Polyhedral type of mesh is used with twelve layers of prism layers near the wall region to capture the right value of y^+ based on the turbulence model and the wall function used, and the total number of elements is approximately 9 million.

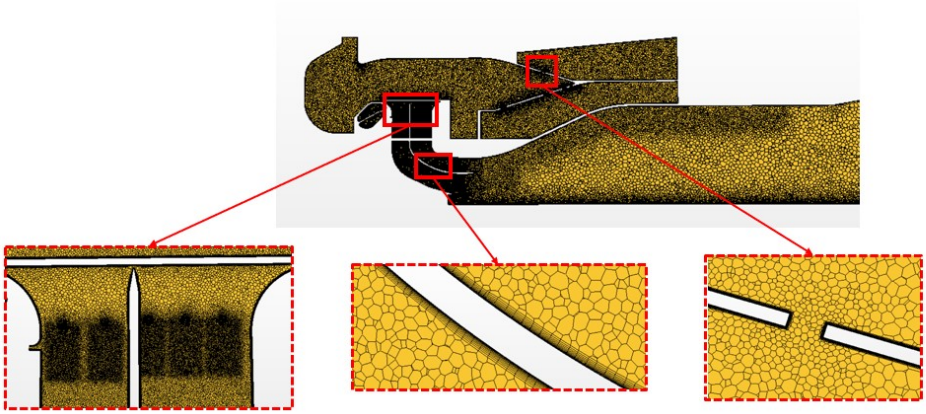

Figure 12: Mesh resolution at different locations in the burner

3.4 Boundary Conditions

Boundary conditions applied to this geometry include periodic boundary conditions in the tangential direction, mass flow and velocity inlets, mass flow outlet, and pressure outlet. The values used for boundary conditions are the values obtained from SGT-750 running at full load conditions, and the normalized data are depicted in table 6. As it is clear from figure 13, air enters the combustion chamber from two boundaries namely, casing and liner, and they are modeled as mass flow inlets with mass flow and temperature values obtained from the compressor outlet. Fuel, on the other hand, enters the chamber from the fuel inlet. To reduce the computational costs, instead of including pilot and RPL in the model, velocity and temperature profiles from the full model are applied to the pilot inlet. On both sides of the thirty-degree model, periodic boundary conditions are applied. The burnt mixture of fuel and air exits the combustion chamber from the main outlet and is modeled as a pressure outlet with a relative value of zero compared to the reference pressure inside the combustion chamber, and at last, in order to consider the leakages in the system, either for fuel or air, a value is deduced from the inlet mass flow rates. As for the physical walls, no slip condition applies to all of them, and since heat transfer is not studied in this work, they are assumed to be adiabatic.

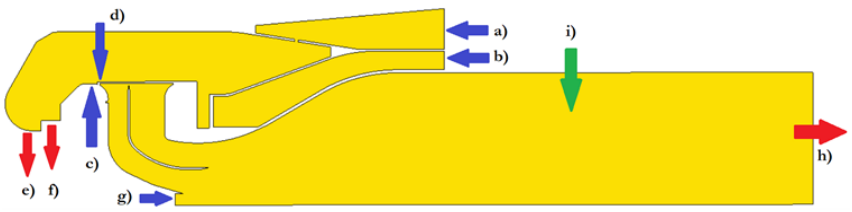

Figure 13: Boundary conditions in the domain, a) air inlet-casing, b) air inlet-liner, c) fuel inlet, d) air leakage inlet, e) pilot outlet, f) air leakage outlet, g) pilot inlet, h) main outlet and i) periodic condition ©M. Safari (2020). Reprinted with permission from the copyright holder.

Table 6: The data for boundary conditions used in the 30 degree sector model

Boundary Names	Type	Normalized Mass Flow Rate [-]	Normalized Temperature [-]
Air inlet_Casing	Mass Flow Inlet	0.264	1
Air inlet_Liner	Mass Flow Inlet	0.775	1
Air inlet_Leakage	Mass Flow Inlet	0.009	1
Fuel inlet 1	Mass Flow Inlet	0.007	0.379
Fuel inlet 2	Mass Flow Inlet	0.018	0.379
Pilot inlet	Velocity Inlet	Velocity Profile from the Full Model	Temperature Profile from the Full Model
Main outlet	Pressure Outlet	-	-
Pilot outlet	Outlet	0.033	-
Air outlet_Leakage	Outlet	0.002	-

3.5 Convergence and Monitoring

As for monitoring the convergence, residuals can be a good indicator of the errors in the flow field, and it is expected to have smooth residuals with low values. However, residuals might not indicate convergence in all locations in the computational domain. Therefore, eight points in the domain, six planes in main channel 1, and seven planes in main channel 2 have been defined as probes, including the outlet of main 1 and main 2. Mass flow rate, velocity magnitude, standard deviation of equivalence ratio, mixture fraction, and temperature are the properties evaluated on these probes.

3.6 Solver Setup

For CFD simulations and sweeping the location of fuel nozzles, STAR-CCM+ and Design Manager are used respectively. As one of the aims of this study is to investigate the stability of three different RANS turbulence models namely, k-ε Realizable, k-ε Lag EB, and k-ω SST, the effects of turbulence have been evaluated, and ultimately one model is chosen for further improvements. Table 7 shows a summary of the setup used in STAR-CCM+.

Table 7: A summary of general solver settings

Solver Setting	Formulation
Solver	Pressure-based
Turbulence models	k-ε Realizable
	k-ε Lag EB
	k-ω SST
Temporal formulation	Steady
Wall treatment	High y^+ wall treatment
Velocity-pressure coupling	Segregated solver
Gas model	Multi-component mixture
Type of flow	Reacting
Turbulent combustion model	Flamelet
Momentum	Second order upwind
Turbulent kinetic energy	Second order upwind
Turbulent dissipation rate	Second order upwind

Design manager uses geometrical parameters defined in STAR-CCM+ as inputs for the improvements. These geometrical parameters are the location of the center of each fuel nozzles in both main channels. The ultimate goal of the improvement

is to achieve a lean well-premixed fuel profile, which is flat in the middle, and lower on the sides near the walls of the burner. This is due to reducing the laminar flame speed in the low-velocity zones, which consequently reduces the possibility of flashbacks in the burner. Furthermore, it is also desirable to keep the standard deviation of equivalence ratio as low as possible at the outlet of main channels 1 and 2. In other words, it is expected to have minimum scattering in the fuel profile to ensure a better mixing occurs in the channels. Equivalence ratio is the property of interest that demonstrates how the fuel-air mixture changes as the location of fuel nozzles are swept along the fuel pipe. Thus, a plot, also known as fuel profile, with equivalence ratio on the vertical axis and the radius from the inner to the outer wall, r, on the horizontal axis is drawn, figure 14B.

To achieve the desirable fuel profile, it is decided to divide the plane located at the outlet of each main channel into four parts. The size of these sections on the planes depends on the reactivity of the fuel used in the burner; however, the portions closer to the inner and outer walls are smaller than the two middle portions. Thereafter, tangential average of equivalence ratio is defined as a response for Design Manager with the objective of minimizing the tangential average of equivalence ratio in the two portions near the inner and outer walls and minimizing the difference of tangential average for the two middle portions of the plane, 14C. However, there are some limitations to sweeping the fuel holes. These limitations include:

- Each fuel nozzle on the fuel pin should be in between the two opposite fuel nozzles on the same fuel pin.
- The fuel nozzles cannot be very close to the walls of the burner.
- The fuel nozzles cannot be very close to each other even though, the achieved fuel profile might seem to be ideal when using RANS. This is due to reducing the errors involved in running RANS models, which later might be figured out while running LES, which is more accurate.

For data presentation, all the values of mass flow rate, velocity, and equivalence ratio have been normalized with the total burner mass flow rate, the average velocity over a plane at the most constricted section, and the global equivalence ratio which is the main outlet's equivalence ratio, respectively. In figures where equivalence ratio is denoted with Low and High, they respectively correspond to the lowest, and highest value of equivalence ratio in main channel 1, and 2 separately in the Baseline Design.

3.7 Mesh Sensitivity Study

Since CFD is a numerical approach, the results can highly depend on the grid generated for the simulation. Therefore, a critical step in CFD simulations is to perform mesh verification or grid independence study. Thus, three different grids have been tested and the results are presented below. As it is clear from table 8, average mass flow rate and standard deviation of equivalence ratio at the outlet of main channel 1 and main channel 2, are chosen as the properties to investigate the grid independence. It is demonstrated that as the grid becomes finer, the difference

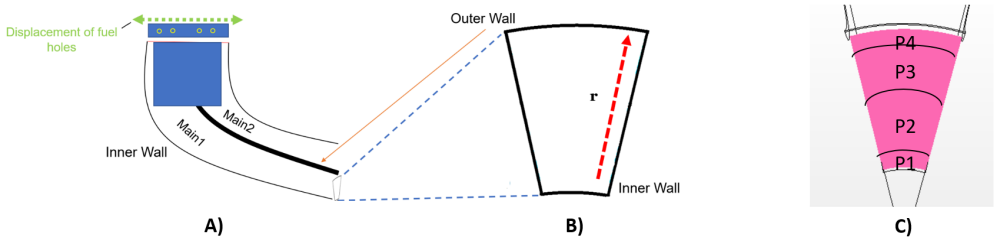

Figure 14: A) Side view of the main channels, B) Plane located at the outlet of main channel 1 ©M. Safari (2020). Reprinted with permission from the copyright holder, C) Divided plane at the outlet of main channel 1

in average mass flow rate and standard deviation of equivalence ratio decreases. This is specifically prominent in the standard deviation of equivalence ratio, such that the difference between 4 million and 9 million grids are immense both at the outlet of main channels 1 and 2; however, the difference between 9 million and 16 million grids is drastically reduced. As for mass flow rate, the difference is so small that the outcome may be influenced by convergence. This might explain why for main 1 mass flow rate, the difference has not changed significantly.

Table 8: The data obtained for grid independence study

Property	4 Million Cells	Difference [%]	9 Million Cells	Difference [%]	16 Million Cells
Average Mass Flow Rate Main 1 [-]	0.355	0.611	0.353	0.313	0.354
Average Mass Flow Rate Main 2 [-]	0.642	0.381	0.645	0.067	0.644
Standard Deviation of ER Main 1 [-]	0.0359	14.3	0.0414	2.44	0.042
Standard Deviation of ER Main 2 [-]	0.0212	24.3	0.0270	5.14	0.028

For further investigation, the velocity and fuel profiles for all three grids have been evaluated. Velocity profiles at the outlet of main channels 1 and 2 show a very good agreement between all three grids (see figure 15); however, the fuel profile is slightly different for all three grids. As it is shown in figure 16 A and B, there are slight differences in both main channels 1 and 2, especially near the wall regions. Figure 16 C and D depict how the tangential average of equivalence ratio differs at low and high radius. It is of importance to note that as the mesh becomes finer, tangential average of equivalence ratio is lower at the low radius and higher at the high radius. This is an important observation that should be taken into consideration when the improvement is performed on the location of the fuel nozzles with a finer mesh. Thus, since it is necessary to maintain a balance between computational costs and accuracy, the grid with 9 million cells is chosen for improvements.

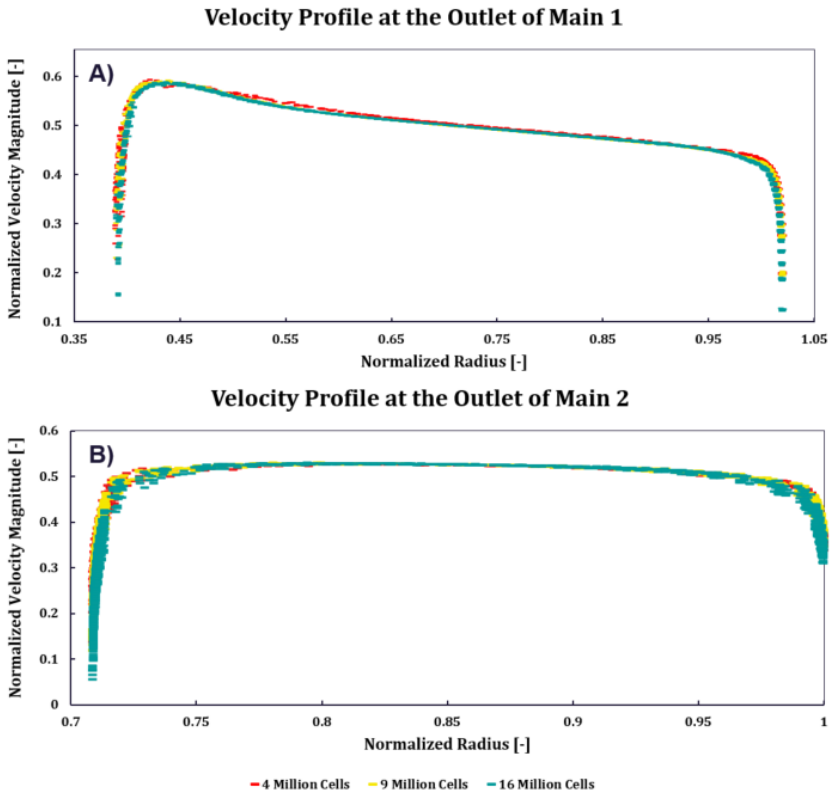

Figure 15: A) Velocity profile at the outlet of main 1 B) Velocity profile at the outlet of main 2

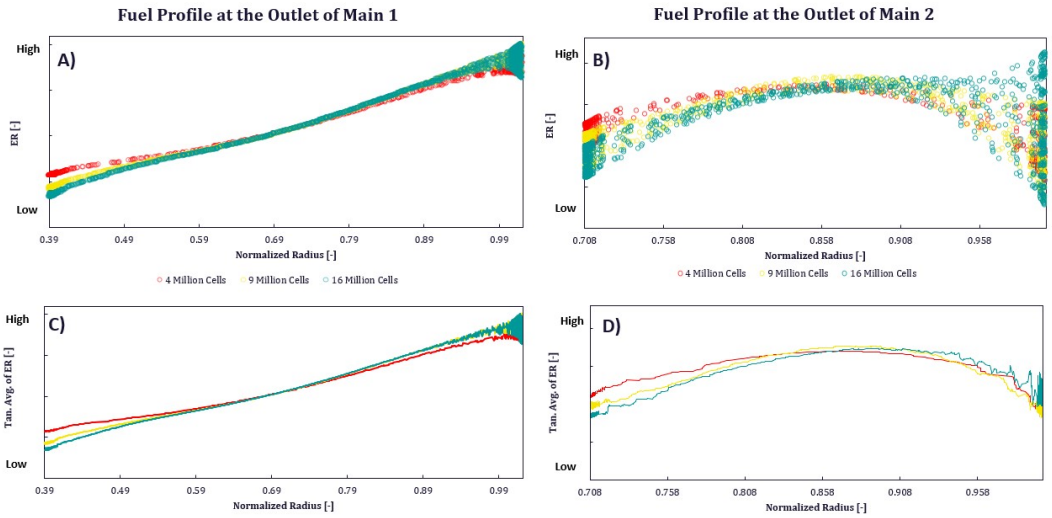

Figure 16: A) Fuel profile at the outlet of main 1 B) Fuel profile at the outlet of main 2 C) Tangential average of equivalence ratio at the outlet of main 1 D) Tangential average of equivalence ratio at the outlet of main 2

4 Results

4.1 Turbulence Models

As mentioned earlier, three RANS turbulence models have been evaluated based on their stability and convergence behavior, and one is chosen for further improvements. Mass flow rate, velocity, standard deviation of equivalence ratio, and temperature are the monitored properties on various probes. As it is clear from figure 17 k-ω SST does not show the desired stability compared to k-ε Realizable and Lag EB both at the outlet of main channels 1 and 2 in predicting mass flow rate, while k-ε Realizable and Lag EB are almost in agreement. This trend is also true with regards to predicting the velocity at the outlet of main channels, figure 18. Although the fluctuations of SST can be negligible in some cases, in this study they can be significant. The instability of the SST model increases, even more, when it comes to standard deviation of equivalence ratio. As it is depicted in figure 19, both k-ω SST and k-ε Lag EB encounter instabilities in predicting the the standard deviation of the equivalence ratio in main channels 1 and 2. Despite the fact that Lag EB fluctuations are much smaller than SST, it can still create non-converged solutions during the improvement phase. Furthermore, figures 20A and B show the convergence for temperature and velocity at a point located in the primary zone of the combustion chamber respectively. In these figures, like figures 17, 18, and 19, k-ε Realizable demonstrates the best convergence behavior, especially in predicting the standard deviation of equivalence ratio, which is a critical factor in the improvement phase. Figures 21 and 22 are the outlet plane in main channel 1 and main channel 2 respectively. It is seen that k-ω SST has a different prediction compared to the k-ε Realizable and Lag EB. Moreover, k-ε Realizable predicts less fuel concentration near the outer wall both in main channels 1 and 2. Thus, it is decided to choose k-ε Realizable model for further investigations and possibly use in the improvement phase. It is worth mentioning that choosing one model does not imply higher accuracy of that model, but they only demonstrate higher stability which can decrease the possibility of non-convergence issues in design iterations.

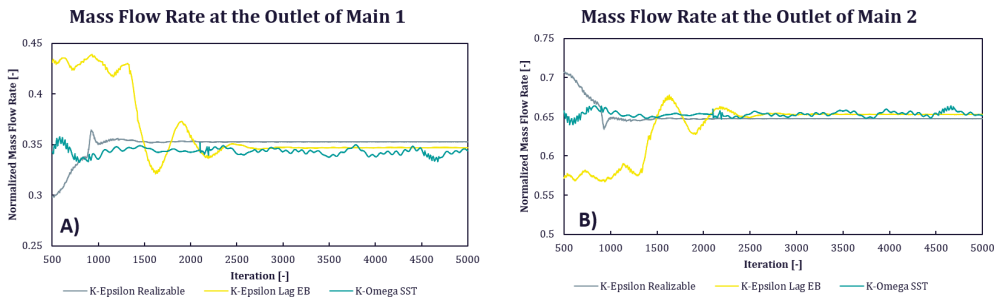

Figure 17: Mass Flow Rate at the Outlet of A) Main 1, B)Main 2 evaluated by three different turbulence models

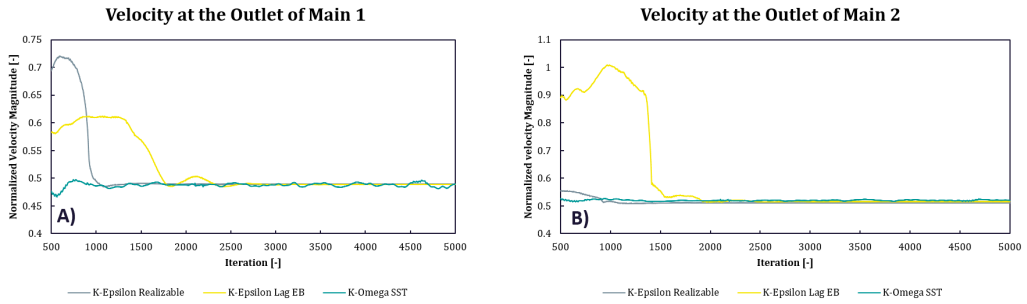

Figure 18: Velocity Magnitude at the Outlet of A) Main 1, B) Main 2 evaluated by three different turbulence models

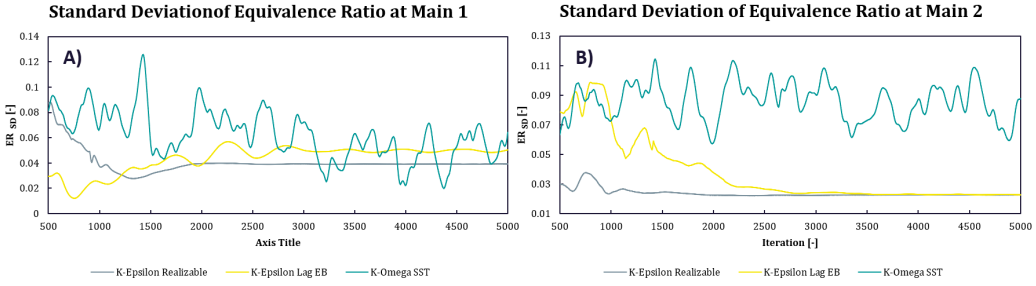

Figure 19: Standard Deviation of Equivalence Ratio at the Outlet of A) Main 1, B) Main2 evaluated by three different turbulence models

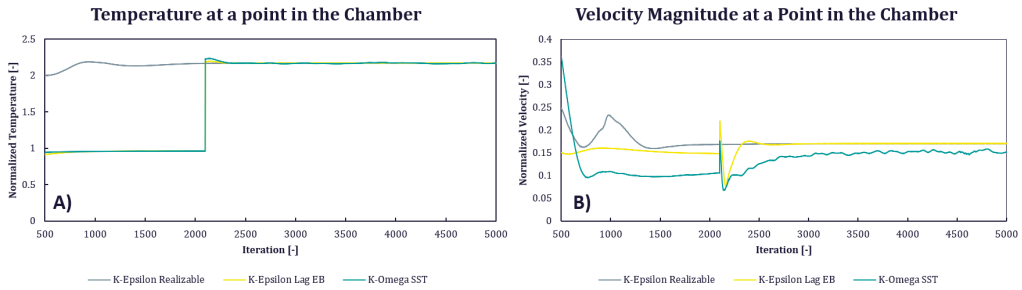

Figure 20: A) Temperature B) Velocity Magnitude at a point in the chamber evaluated by three different turbulence models

4.2 Geometrical Improvements

In this section, the results of the geometrical improvement of fuel-nozzle locations in both main channel 1 and main channel 2 are presented. It is demonstrated how the implemented approach of dividing the outlet plane of main channels into four pieces and minimizing the tangential average of equivalence ratio near the inner and outer walls have helped reduce the fuel concentrations near the walls leading to decreasing the possibility of flashbacks for highly reactive fuels. Furthermore, it is also shown how minimizing the difference between the tangential average of equivalence ratio in the two middle portions of the plane, leads to a more well-mixed mixture of

fuel and air resulting in lower local high-temperature points and thus, lower NOx emissions. Four designs have been presented in this section for main channel 1 and main channel 2, and it is tried to ultimately choose one design in each main channel. The differences between the presented designs for main channel 1 and 2 are measured relative to the center of the fuel nozzles in the Baseline Design. With each design, it is tried to reduce the distance between the fuel nozzles and compact them towards the center of the fuel pin such that the Baseline Design has the largest gap between the fuel nozzles and they are distributed spaciously on the fuel pin, and Design 3 has the least spacing between the fuel nozzles, and they placed toward the center of the fuel pin.

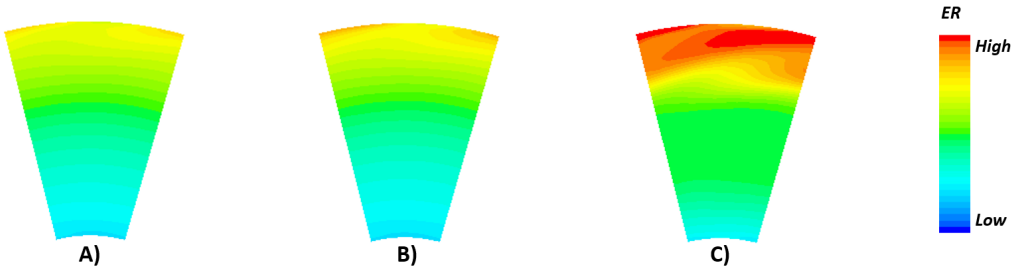

Figure 21: The outlet plane of main channel 1 for A) k-ε Realizable B) k-ε Lag EB, and C) k-ω SST

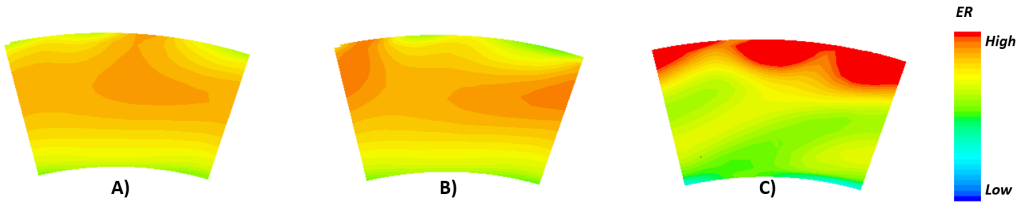

Figure 22: The outlet plane of main channel 2 for A) k-ε Realizable B) k-ε Lag EB, and C) k-ω SST

4.2.1 Main Channel 1

Figure 23 demonstrates the fuel profile for Baseline design and Design 1 at the outlet of main channel 1. As it is clear, the equivalence ratio near the inner wall of main channel 1 is very low for the baseline design which decreases the possibility of flashbacks. However, near the outer wall of main channel 1, the equivalence ratio is much higher than the center of the fuel profile for the Baseline Design. In order to rectify this issue, Design 1 is introduced, which overall has a more flat fuel profile which is ideal in terms of how well-mixed the mixture is. Despite the flat fuel profile, this design is suffering from a higher equivalence ratio value near the inner wall of the channel which may lead to flashbacks into the burner. To eliminate the shortcomings of Design 1 and get closer to the ideal design, Design 2 which has a lower equivalence ratio near the inner wall has been evaluated, figure 24. This design has the advantage of a relatively lower equivalence ratio near the outer wall

compared to the baseline design, despite its higher value in the center of the profile, figure 24. However, Design 3 as the final design for main channel 1 has the best of all the other designs. As it is shown in figure 24, this design has a lower fuel concentration near both walls, compared to the center of the profile, leading to a lower chance of flashbacks in the burner, while it has a relatively flat fuel profile in the middle of the channel demonstrating a well-mixed mixture of fuel and air resulting in lower NOx emissions.

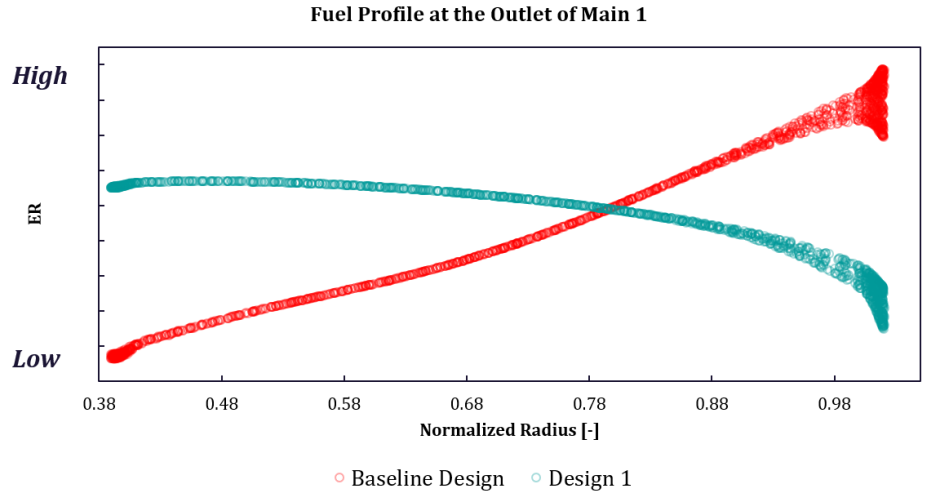

Figure 23: Fuel profile for the Baseline Design, and Design 1 at the outlet of main channel 1

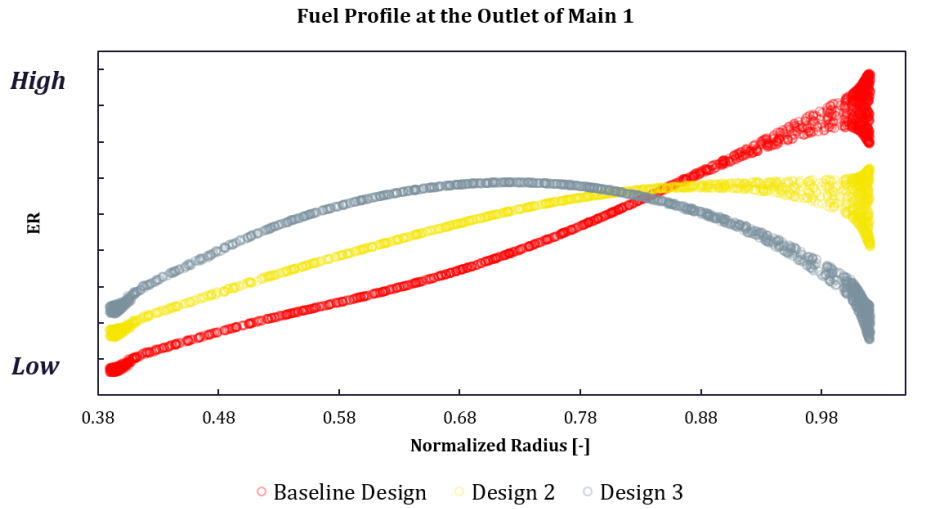

Figure 24: Fuel profile for the Baseline Design, Design 2, and Design 3 at the outlet of main channel 1

Figures 25 to 28 demonstrate the planes located in the streamwise direction in main channel 1 for all designs. Figures A show all the planes located in the main channel, while figures B show only the top planes, focusing on the recirculation zone. Figure 25 shows how the fuel and air are not properly mixed near the inner wall of

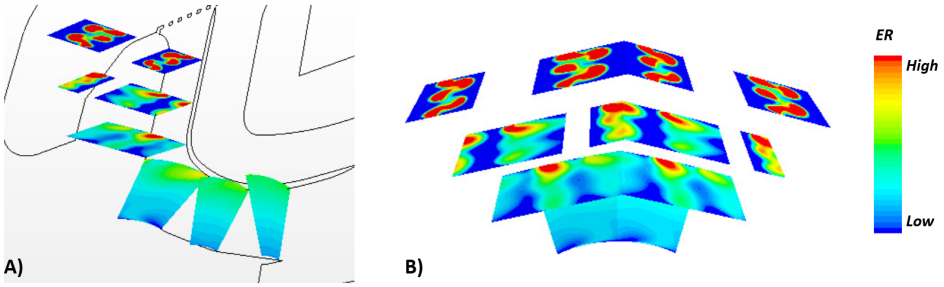

Figure 25: Equivalence Ratio for the Baseline Design in main channel 1 A) in the streamwise direction, B) from the top view for the 60 degree model (mirrored view of the 30 degree model)

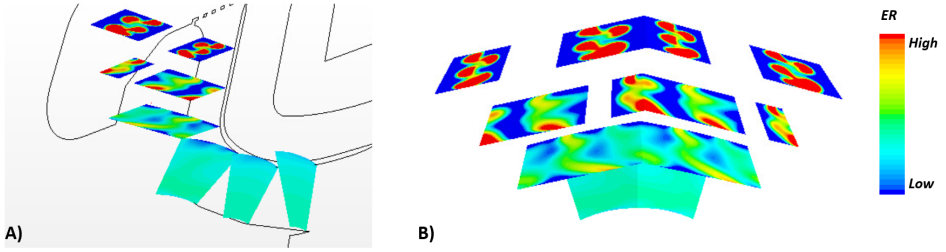

Figure 26: Equivalence Ratio for Design 1 in main channel 1 A) in the streamwise direction, B) from the top view for the 60 degree model (mirrored view of the 30 degree model)

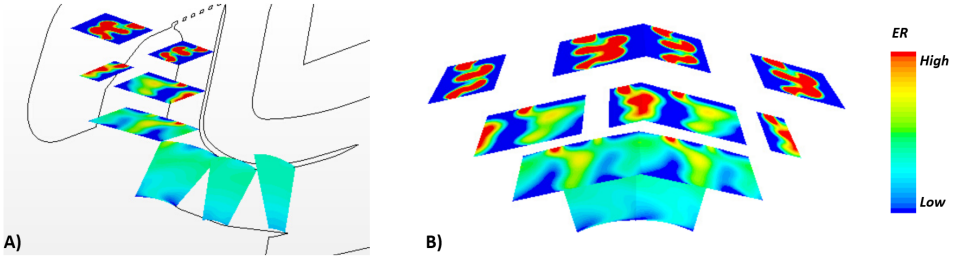

Figure 27: Equivalence Ratio for Design 2 in main channel 1 A) in the streamwise direction, B) from the top view for the 60 degree model (mirrored view of the 30 degree model)

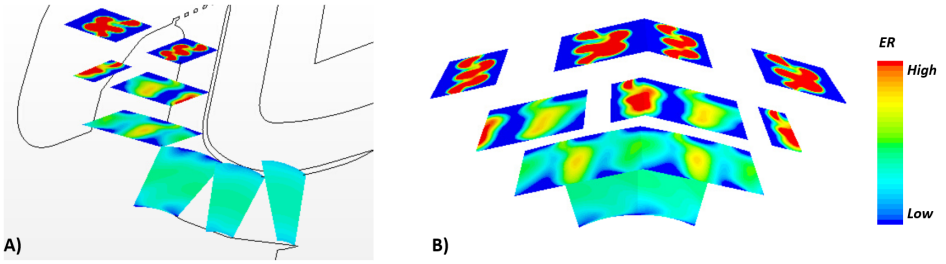

Figure 28: Equivalence Ratio for Design 3 in main channel 1 A) in the streamwise direction, B) from the top view for the 60 degree model (mirrored view of the 30 degree model)

Table 9: The values of tangential average of equivalence ratio in main channel 1 for each segment of the divided plane, and SDER for the whole plane

	Tan. Avg. P1 [-]	Tan. Avg. P2 [-]	Tan. Avg. P3 [-]	Tan. Avg. P4 [-]	Tan. Avg. (P2-P3) [-]	SDER [-]
Baseline Design	0.6240	0.6931	0.8044	0.9060	0.1112	0.0414
Design 1	0.8211	0.8115	0.7757	0.7120	0.0347	0.0175
Design 2	0.6757	0.7544	0.8163	0.8199	0.0622	0.0223
Design 3	0.7247	0.8132	0.8099	0.7230	0.0036	0.0201

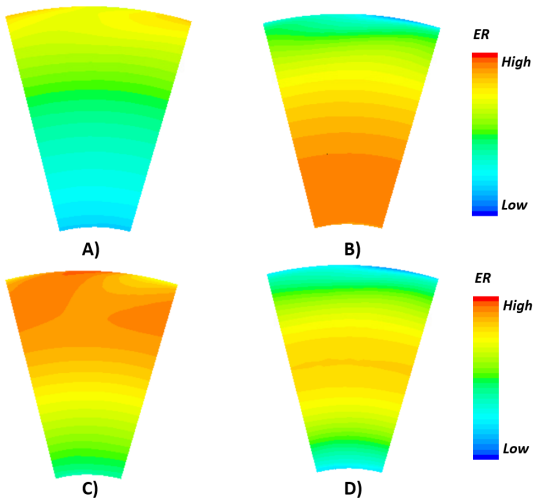

Figure 29: Equivalence ratio at the outlet of main channel 1 for A) Baseline Design B) Design 1 C) Design 2 D) Design 3

main channel 1 in the Baseline Design. Six planes have been placed in the streamwise direction of the flow, and they illustrate that there is a low fuel concentration near the inner wall leading to an undesirable fuel profile seen in figure 23. However, the mixing near the outer wall becomes more homogeneous as seen in the last two planes in figure 25a. Figure 25b shows how fuel and air become more homogeneous right after the swirl wing due to the existence of the recirculation zone. Figures 26 and 27 show the fuel and air mixing in main channel 1 for Designs 1 and 2 respectively. Like figure 25, fuel and air mixing are different near the walls compared to the center of the planes where regions in red have higher fuel concentrations compared to the regions in blue. Figure 26 shows more desirable mixing near the inner wall throughout the channel, while the equivalence ratio is on the low side near the outer wall. Figure 27a demonstrates how the equivalence ratio near the inner wall, after the performed improvement, is still on the low side compared to the outer wall. Similar to figure 25b, figures 26b, and 27b depict the mixing behavior right after the recirculation zone. Figure 28 depicts how the change in the location of fuel nozzles in Design 3 can have a significant impact on the premixing of fuel and air throughout the channel. As it is clear from the top plane in figure 28b, closer placement of the fuel nozzles towards the middle of the channel, led to higher fuel concentrations in the middle of the outlet plane seen in figure 28b in Design 3. Figure 29 demonstrates the fuel concentration at the outlet of main channel 1 for all four designs. It is seen that Design 3 has a much better fuel distribution compared to the Baseline and the other designs.

As mentioned before, the approach considered for evaluating the ideal fuel profile

was to divide the outlet planes in the main channels into four pieces. As it is shown in table 9, Design 3 which is closest to the ideal design, has the lowest difference in tangential average of equivalence ratio between the two middle planes, while the tangential average of equivalence ratio is at a relatively low value for the two side planes.

In all of the designs presented for main channel 1, it is noticed that the scattering is very low, which is crucial in terms of NOx emissions. This is also noticed by checking the value of the standard deviation of equivalence ratio in table 9. It is witnessed that Design 1 and Design 3 are the best choices in terms of lower scatter in the fuel profile followed by Design 2 and the Baseline Design.

4.2.2 Main Channel 2

Three designs have been presented along with the Baseline design for main channel 2. The aim of obtaining different designs is to have higher fuel concentration at the center of the outlet plane in main channel 2, and lower fuel concentration near the inner and outer wall. Figure 30 shows the fuel profile for the Baseline Design and Design 1 at the outlet plane of main channel 2. It is clear from the graph that the Baseline Design already has a flat fuel profile which is ideal in terms of how well-mixed the mixture is. Furthermore, the Baseline design can be acceptable if natural gas is used as a fuel since it is not highly reactive and thus, there is no risk of flashbacks. However, in an attempt to reduce the fuel concentrations near the walls, Design 1 is introduced which has a lower equivalence ratio near the outer wall. This design has two disadvantages including a higher equivalence ratio near the inner wall, and scattering near the outer wall, where the maximum value indicates increased risk of wall flashbacks. Consequently, Designs 2 and 3 are used to rectify the shortcomings of Design 1, figure 31. As it is demonstrated in figure 31, Designs 2 and 3 are very similar in results and both are very close to the ideal design for highly reactive fuels. However, Design 3 has slightly higher values of equivalence ratio in the middle of the plane and lower values of equivalence ratio near the inner and outer walls. This is also well-indicated in table 10 that the tangential average of equivalence ratio in P1 and P4 are lower in Design 3 compared to Design 2. From this table, it is also noticed that the Baseline Design still has the lowest difference between the two middle portions of the planes compared to the other designs.

Figures 32, 33, 34, and 35 are the contours of equivalence ratio for the Baseline Design, Design 1, Design 2, and Design 3 respectively. These figures demonstrate how the fuel and air mixing occurs throughout main channel 2, while the regions in red have the highest fuel concentration and regions in dark blue have the lowest fuel concentration. Like main channel 1, figures A depict planes located throughout the channel to better show the mixing behavior, while figures B focus on the recirculation zone. Figure 32a show that the Baseline Design has a uniform fuel distribution, specially at the outlet of the channel. Moreover, figure 32b shows right after the swirl wing, the mixture of fuel and air starts to become more homogeneous. Design 2 and 3 which demonstrated a better behavior in terms of fuel profile also show a better mixing behavior in these figures compared to Design 1. It is especially seen that for these two designs, the middle of the plane has a higher equivalence ratio, while near the walls, there are regions with lower equivalence ratio values.

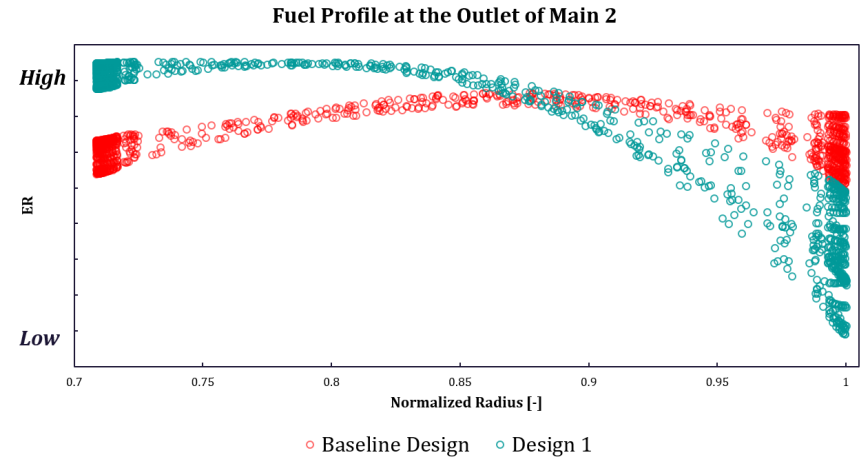

Figure 30: Fuel profile for the Baseline Design, and Design 1 at the outlet of main channel 2

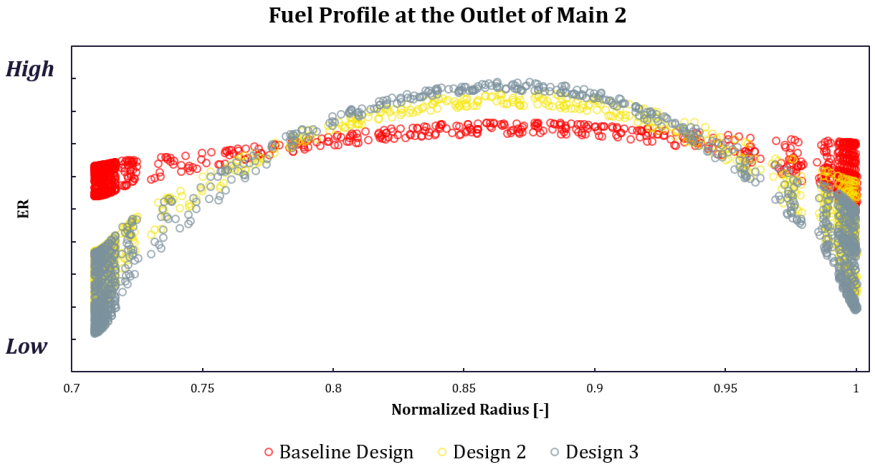

Figure 31: Fuel profile for the Baseline Design, Design 2, and Design 3 at the outlet of main channel 2

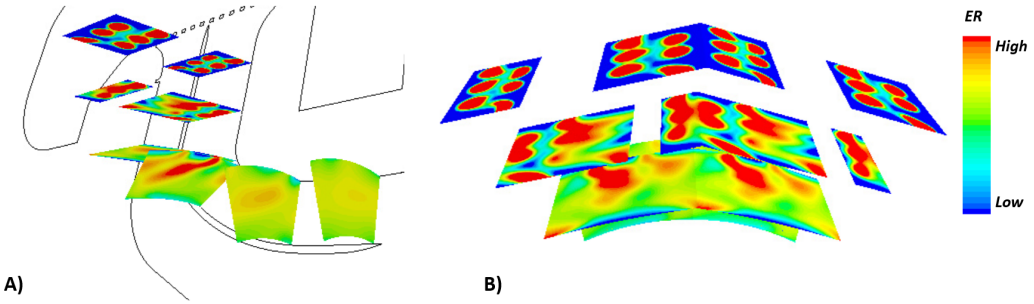

Figure 32: Equivalence Ratio for the Baseline Design in main channel 2 A) in the streamwise direction, B) from the top view for the 60 degree model (mirrored view of the 30 degree model)

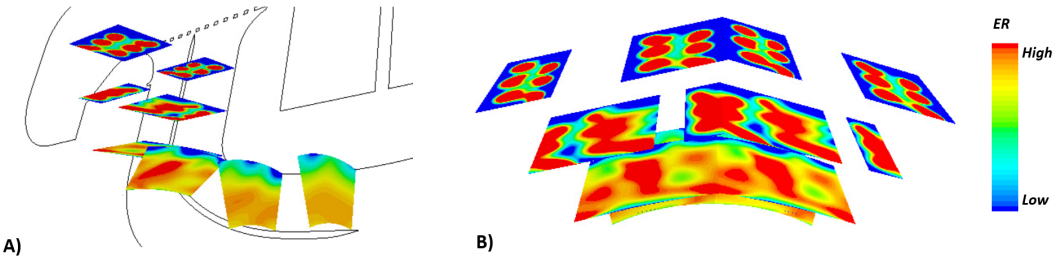

Figure 33: Equivalence Ratio for Design 1 in main channel 2 A) in the streamwise direction, B) from the top view for the 60 degree model (mirrored view of the 30 degree model)

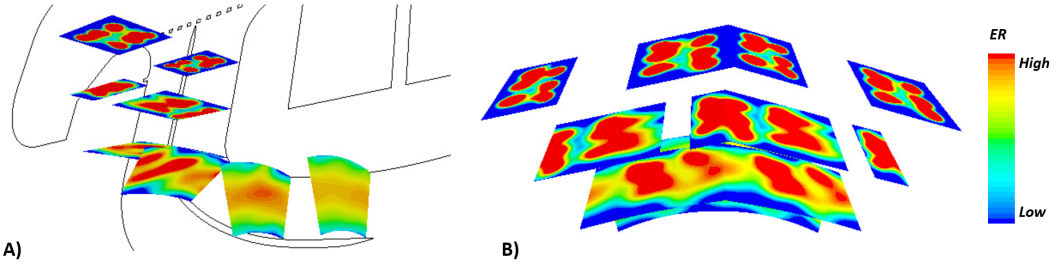

Figure 34: Equivalence Ratio for Design 2 in main channel 2 A) in the streamwise direction, B) from the top view for the 60 degree model (mirrored view of the 30 degree model)

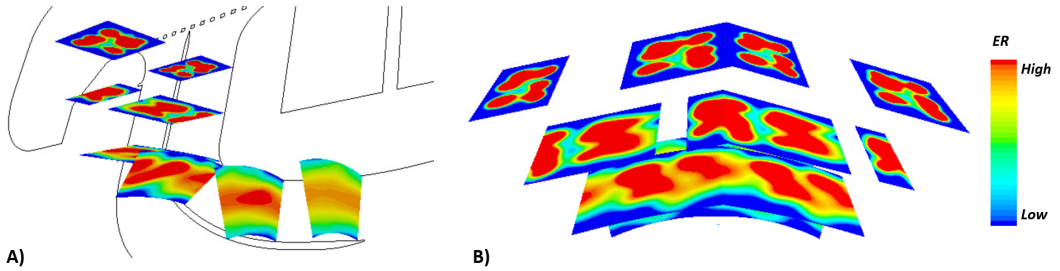

Figure 35: Equivalence Ratio for Design 3 in main channel 2 A) in the streamwise direction, B) from the top view for the 60 degree model (mirrored view of the 30 degree model)

As it is seen in figures 34a, and 35a, until half way through the channel, there are regions with high fuel concentrations, specially in the middle of the channel showing that the premixing is not completed. By the same token, 34b, and 35b, completely depicts that right after the swirl wing there is more of a uniform pattern of fuel and air despite not being mixed properly. This repetitive pattern of fuel concentration in the radial direction of the burner right after the swirl wing, can be one of the reasons that Design 2 and 3 demonstrate ideal fuel profiles at the outlet of main channel 2. Figure 36 depicts the outlet of main channel 2 for all four designs. It is observed that, like the fuel profiles, Design 3 has the most ideal fuel distribution compared to the other designs for highly reactive fuels, while the Baseline Design is most suitable for less reactive fuels. As for scattering in the fuel profile in main

channel 2, Design 1 and Design 3 have the highest scatter, and thus, higher values of standard deviation of equivalence ratio as shown in table 10, while the best design in terms of scattering is the Baseline Design.

Table 10: The values of tangential average of equivalence ratio in main channel 2 for each segment of the divided plane, and SDER for the whole plane

	Tan. Avg. P1 [-]	Tan. Avg. P2 [-]	Tan. Avg. P3 [-]	Tan. Avg. P4 [-]	Tan. Avg. (P2-P3) [-]	SDER [-]
Baseline Design	1.0574	1.1447	1.2231	1.0847	0.0784	0.0270
Design 1	1.2911	1.2908	1.1549	0.8400	0.1359	0.0855
Design 2	0.9153	1.2012	1.2702	1.0196	0.0690	0.0692
Design 3	0.8768	1.2303	1.2996	0.9854	0.0693	0.0852

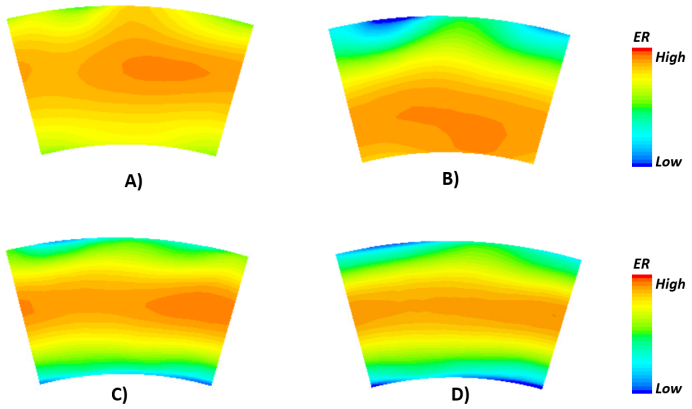

Figure 36: Equivalence ratio at the outlet of main channel 2 for A) Baseline Design B) Design 1 C) Design 2 D) Design 3

5 Discussion

5.1 Turbulence Models

Among all three turbulence models evaluated, namely, k-ε Realizable, k-ε Lag EB, and k-ω SST, k-ε Realizable had the best convergence stability in all the properties on all the probes located throughout the computational domain. Since the improvement phase contains comparisons between many similar cases, it is very important to obtain a well-converged solution to eliminate the wrong conclusion due to non-convergence. Hence, k-ε Realizable is chosen for the improvements on the fuel-nozzle locations. However, it is not clear how accurate this turbulence model is in the conducted simulations, and it is crucial to run more accurate simulations such as LES or experimental studies, to evaluate the accuracy of the models. If such a study would show that the used RANS model deviates in a certain way, then the geometry improvement should be repeated with this deviation in mind. In the end, it is recommended to perform LES or experiments again to confirm the outcome.

When comparing the outlet plane of main channels for equivalence ratio in figures 21 and 22, k-ε Realizable and Lag EB are similar, except near the outer wall region where Lag EB predicts a bit more fuel concentration. This is also consistent with figure 19A in which Lag EB over-predicts the values of SDER compared to Realizable. On the other hand, k-ω SST demonstrates convergence issues on all the probes in the domain, and thus the contours on the outlet planes of both main channels are very different and unreliable compared to both Realizable and Lag EB. Nevertheless, this behavior of k-ω SST might be because of oscillatory convergence due to the flow field being highly unsteady, and it can be resolved by sampling over a large number of iterations and taking an average. These findings are in complete agreement with the findings of Charoenchang on the jet in crossflow study, where she concluded that k-ε Realizable and LES are acceptable and accurate models for predicting the flow behavior, while k-ε Lag EB and k-ω SST are not suitable for this study [15].

One of the methods that could rectify the convergence issues encountered while running k-ω SST could be by running unsteady simulations. Charoenchang in her thesis understood that by running unsteady k-ω SST the solution could converge; however, the results still deviated from LES and experimental data [15]. It is worth mentioning that for the point located in the chamber, k-ω SST predicts the temperature and the velocity quite accurately with minor fluctuations.

As for all turbulence models it is highly recommended to check the swirl number, which is the ratio of the axial flux of angular momentum to the axial flux of linear momentum, at each plane in the main channels to understand the effects of axial and lateral velocities on premixing. This can consequently indicate the influence of swirl number on both equivalence ratio and mass flow rate. Another parameter that can be significant and is advised to check for further studies is the turbulent kinetic energy.

5.2 Improvements on Fuel Nozzle Locations

Since meshing is one of the most critical steps in CFD simulations, it is believed that some errors are introduced in the results due to meshing. One of the most critical issues with meshing is to capture the flow behavior near the physical walls by using prism layers. However, controlling the thickness of prism layers throughout the entire computational domain can be challenging. Although the chosen prism layers satisfied the y^+ value in the main channels, the y^+ value in the chamber, despite its negligible effect on the premixing, could have exceeded the desired value. Another potential factor that influenced the results, especially the premixing in the main channels, was the sudden change in the size of mesh used for the volumetric mesh refinement, and the free-stream mesh. This might have resulted in certain flow behavior not being completely captured, neither in choosing the turbulence model nor in the investigation of the fuel profiles. Since only a portion of the combustion chamber of SGT-750 was modeled to reduce the computational costs, a higher number of cells could be dedicated to the regions were of prime importance. Despite the uncertainties brought to the simulations, in this case, the advantages outweigh the disadvantages.

There can be some other sources of errors involved in the obtained results as well. One of these errors can mainly originate from the assumptions made to simplify the problem. Reducing the full model to a thirty-degree portion of the model with periodic boundary conditions on the sides and other similar assumptions have definitely contributed to the errors involved in the simulations. By using periodic boundary conditions, it is expected that the flow has a periodically repeating nature, while this might not be exactly the case. Another assumption was not including the pilot and RPL for the simulations, however, this assumption is thought to introduce negligible errors on the premixing that takes place in the main channels. Furthermore, the models used such as steady-state simulations to shorten the time of the simulations or using the flamelet model which is a simplified model could also have added to the errors. Nevertheless, in the absence of LES or experimental data for this study, it cannot be claimed that the errors have affected the results significantly.

Design manager has been used for sweeping the location of fuel nozzles which resulted in some new designs for both main channel 1 and main channel 2. Design 3 has been shown to be the best design based on the mentioned criteria for main channel 1. Since it was decided that the two middle portions, occupy most of the area of the outlet plane in main channel 1, a flat fuel profile in the middle of the main channel 1 means very little difference between the middle portion's tangential average of equivalence ratio, compared to the sides. Based on table 9, the tangential average of equivalence ratio for the near-the-wall portions of the outlet plane is much larger than the difference between the two middle portions. Thus, it is clear that this fuel profile is very close to the ideal fuel profile. However, it is noticed that lower values of ER than the flammability limit near the walls result in a parabolic fuel profile which is not completely ideal in terms of NOx emissions since it shows a non-well-mixed mixture of fuel and air, and this leads to local high-temperature regions, even though it is highly desirable in terms of wall flashback point of view for highly reactive fuels. It was noticed that as the fuel nozzles got closer to the center of the fuel pin, the fuel profile also got closer to an ideal fuel profile.

As for main channel 2, it is noticed that the Baseline design is most suitable for fuels that are not highly reactive such as natural gas, due to a flat fuel profile demonstrating proper mixing in the channel, while Design 3 depicts the best behavior for highly reactive fuels such as Hydrogen due to the parabolic shape of the fuel profile. Same as main channel 1, the difference between the middle portions of the outlet plane in main channel 2 is in a lower order than the values of the tangential average of equivalence ratio near the walls for all the designs, demonstrating that even Design 3 is still a good option among all the designs for highly-reactive fuels. Nonetheless, scattering near the walls in main channel 2 is higher than main channel 1 as seen in figures 30 and 31. Since the change in the designs in main channel 2 is the same as main channel 1 such that the fuel nozzles have got closer to the center of the fuel pin, with Design 3 demonstrating the closest they get, the concentration of fuel decreases near the walls, and thus, it may lead to higher scattering at the outlet of main channel 2. From figure 31, it is also clear that when comparing the Baseline design and Design 3, in the middle of channel where higher fuel concentration exists for Design 3, the scattering is also less.

The changes in the location of fuel nozzles have been the same on both of the fuel pins. Thus, slight adjustments on each fuel pin separately could lead to significant changes. Separate changes on the fuel pins can be performed by considering the effects of the guide vane located under the fuel pins. From Safari's study, it is known that the jet on the right side of the guide vane is different from the jet left side of the same vane [14]. Thus, this could be an advantage to adjust the fuel nozzles on each fuel pin separately to achieve the desired fuel profile. Moreover, some restrictions on fuel-hole locations were inserted due to utilizing RANS, which could significantly affect the results. Moreover, it was decided to limit the number of variables for the improvement phase such that the computational costs would be reasonable. The only parameter that could vary throughout the improvement phase was tangential movement of the fuel nozzles. Thus, if fuel nozzles have more degrees of freedom, better results might be obtained. Furthermore, the diameter of the holes was also kept constant, while the change in this parameter can significantly influence the improvements done.

6 Conclusions

The main objective of this study was to improve the tangential location of fuel nozzles located on the fuel pins above main channel 1 and main channel 2 in the SGT-750 prototype burner. The motivation of this study was to obtain a fuel profile that is flat in the middle and lower in the near wall regions such that if highly reactive fuels are used, the risk of flashbacks in the burner is minimized. A flat fuel profile also eliminates fuel concentrations leading to the elimination of local high-temperature points, and thus less NOx emissions. The above objectives should be attained by trying to keep the scattering in the fuel profile as low as possible.

In order to obtain the fuel profile, a plane is located normally in the streamwise direction at the outlet of main channel 1 and main channel 2, and the equivalence ratio is evaluated as a function of radius based on the burner axis. The approach for the improvement was to divide the plane located at the outlet into four parts and minimize the difference between the tangential average of equivalence ratio in the two middle portions of the outlet plane contributing to the flat part of the fuel profile, and minimizing the tangential average of equivalence ratio in the near the wall portions.

The software used for the CFD simulations was Star-CCM+, and Design Manager was used for sweeping the fuel nozzles in the tangential direction. In order to make the simulations less computationally expensive, some assumptions and simplifications were made such as only considering a thirty-degree slice of the full burner. Three different grids were generated to investigate the effects of the grid on the solution, and it was found that as the grid becomes finer, the tangential average of equivalence ratio is lower at lower radius, and higher at higher radius compared to the coarser grids in the main channels. Since the most severe difference between the middle grid and the finest grid was around five percent, which is for the standard deviation of equivalence ratio at the outlet of main channel 2, it was decided that the middle grid possesses enough accuracy for this study.

Since part of the scope of this study was to evaluate the most stable RANS model in combination with the FGM model for this case, three turbulence models namely, k-ε Realizable, k-ε Lag EB, and k-ω SST, were evaluated and it was found that k-ε Realizable, from convergence point of view performed much better than the other two models. k-ε Lag EB on the other hand, demonstrated stability for all the criteria except the standard deviation of equivalence ratio at the outlet of main channel 1. Therefore, k-ε Realizable was chosen for the improvement phase of this study.

Three designs were presented in the improvement phase apart from the Baseline Design to find the most suitable design that satisfies the mentioned criteria. It was found that in main channel 1, Design 3 was the closest to the ideal fuel profile. It was also noticed that the value of standard deviation of equivalence ratio for almost all designs in main channel 1 was low, which means they did not suffer much from scattering. Design 3 is the design in which the fuel nozzles are placed closest to each other near the center of the fuel pin above main channel 1. This design still satisfies the limitation put in place for choosing the best design from section 3.6.

Among the evaluated configurations, two separate designs were obtained for main channel 2, depending on the application. It was found that the Baseline Design was the most suitable design for when non-highly reactive fuels are used. On the other hand, Design 3 with lower fuel concentration near the wall regions was the most suitable choice for highly reactive fuels such as Hydrogen. The chosen designs, like the improvement performed in main channel 1, satisfy the conditions of section 3.6.

7 Outlook

Due to the limitations and lack of time, the scope of this thesis was restricted to only evaluating the effects of movement of the fuel nozzles along the fuel pins. Thus, the following points can be investigated to fully achieve the best possible fuel profile.

- The number and the diameter of fuel nozzles were assumed to be constant due to the design limitations such as combustion dynamics issues. However, one possibility is to decrease the number of nozzles on the fuel pin. This limitation could affect the mixing near the walls of the channels as well as the center of the profile. This also could influence the scattering in the fuel profile. Therefore, it is recommended to investigate this possibility in the design of the fuel pins.
- Since none of the turbulence models was validated to ensure they can accurately predict the mixing, it is highly recommended before conducting further improvements and simulations, LES would be run to quantify the deviations between LES and RANS. This should then be taken into account during further design improvements.
- Finally, the outcome of the simulations should be proven by high pressure tests to evaluate the performance of the improved design for the reduced NOx emission and flashback resistance.

8 Perspectives

This thesis work primarily focused on providing a better mixture of fuel and air in the main channels of the SGT-750 gas turbine engine to reduce NOx emissions which is one the most important pollutants from gas turbines. Moreover, this thesis succeeded in offering a design that not only reduces NOx emissions but also reduces the risk of flashbacks into the burner, leading to safely utilizing highly reactive green fuels such as hydrogen.

References

[1] Bender W. Lean premixed combustion. Technology & Management Services. Inc, Gaithersburg, MD. 2007;20879.

[2] Cox L. Nitrogen oxides (NOx) why and how they are controlled. Diane Publishing; 1999.

[3] Stansel D, et al. Gas Turbine Emissions Improvements by Advances in Design, Analysis, Materials, Manufacturing, and Control Technology. In: Proceedings of the 47th Turbomachinery Symposium. Turbomachinery Laboratory, Texas A&M Engineering Experiment Station; 2018. .

[4] Caracciolo L, Rubini P. Validation of a Partially-Premixed Combustion Model for Gas Turbine Applications. In: Turbo Expo: Power for Land, Sea, and Air. vol. 42363; 2006. p. 731-42.

[5] Nilsson EJ, Brackmann C, Abou-Taouk A, Larfeldt J, Moell D. Hydrogen Addition to Flames at Gas-Turbine-Relevant Conditions. Energiforsk Report. 2017.

[6] Sadykova SB, Dostiyarov AM, Zhumagulov MG, Kartjanov NR. The influence of turbulence on the efficiency and reliability of combustion chamber of the gas turbine. Thermal Science. 2021;(00):64-4.

[7] Stefanizzi M, Capurso T, Filomeno G, Torresi M, Pascazio G. Recent Combustion Strategies in Gas Turbines for Propulsion and Power Generation toward a Zero-Emissions Future: Fuels, Burners, and Combustion Techniques. Energies. 2021;14(20):6694.

[8] Motsamai OS, Snyman JA, Meyer JP. Optimization of gas turbine combustor mixing for improved exit temperature profile. Heat transfer engineering. 2010;31(5):402-18.

[9] Siemens in India;. Available from: `http://w4.siemens.de/archiv/en/laender/asien/indien.html` [cited 04.03.2022].

[10] SGT-750 Gas Turbine Engine;. Available from: `https://press.siemens.com/global/de/pressemitteilung/siemens-baut-fokussierten-energieriesen-und-steigert-leistungsfaehigkeit-weiter` [cited 04.03.2022].

[11] Koren D. Computational Fluid Dynamics Unstructured Mesh Optimization for the Siemens 4th Generation DLE Burner; 2015.

[12] Lindfors J. Performance of cracked ammonia combustion in a gas turbine engine-Evaluation through CFD and chemical reactor network modeling. 2022.

[13] Benim AC, Syed KJ. Flashback mechanisms in lean premixed gas turbine combustion. Academic press; 2014.

[14] Safari M. Geometrical improvement of SGT-750 burner; 2020.

[15] Charoenchang W. Analysis of Fuel-Air Mixing in Jet in Crossflow. 2021.

[16] Saravanamuttoo HI. Gordon Frederick Crichton Rogers, and Henry Cohen. Gas Turbine Theory. Pearson Education, Harlow, Essex; 2001.

[17] Moell D. Modelling of methane and hydrogen enriched methane flames in industrial gas turbine burners. Lund University, Faculty of Engineering; 2018.

[18] El-Sayed AF. Aircraft propulsion and gas turbine engines. CRC press; 2017.

[19] Brayton Cycle;. Available from: https://en.wikipedia.org/wiki/Gas_turbine#/media/File:Brayton_cycle.svg [cited 04.03.2022].

[20] Brun K, Kurz R. Introduction to Gas Turbine Theory: An Overview of Fundamental Concepts. Solar Turbines Incorporated; 2004.

[21] Cleynen O. Different types of gas turbine engines;. Available from: https://en.wikipedia.org/wiki/Gas_turbine#/media/File:Gas_turbine_applications_(numbered).svg [cited 04.03.2022].

[22] Benini E. Progress in gas turbine performance. BoD–Books on Demand; 2013.

[23] Shrivastava A, Patel VK. Effect of injection angle of primary and secondary holes on the mixing and combustion in a can type combustor using CFD. SN Applied Sciences. 2019;1(7):1-13.

[24] Royce R. The jet engine. Rolls-Royce plc; 1996.

[25] Igoe B. Dry low emissions experience across the range of Siemens small industrial gas turbines. Siemens Industrial Turbomachinery Limited, Lincoln, UK. 2011.

[26] Reddy UC, Blanchard CE, Schlein BC. FT8-3 Advanced Low Emissions Combustor Design. In: Turbo Expo: Power for Land, Sea, and Air. vol. 43970; 2010. p. 1337-43.

[27] Boyce MP. Gas turbine engineering handbook. Elsevier; 2011.

[28] Kurdyumov V, Fernandez E, Linan A. Flame flashback and propagation of premixed flames near a wall. Proceedings of the Combustion Institute. 2000;28(2):1883-9.

[29] SGT-750 4th Generation Burner;. Available from: https://www.siemens-energy.com/global/en/offerings/power-generation/gas-turbines/sgt-750.html#:~:text=The%20SGT%2D750%20is%20a,heavy%2Dduty%20industrial%20gas%20turbine [cited 04.03.2022].

[30] SGT-750 Gas Turbine Engine;. Available from: https://www.siemens-energy.com/global/en/offerings/power-generation/gas-turbines/sgt-750.html#:~:text=The%20SGT%2D750%20is%20a,heavy%2Dduty%20industrial%20gas%20turbine. [cited 04.03.2022].

[31] Hellberg A. The Siemens SGT-750 Gas Turbine: Developed for the Oil and Gas Industry. Rep Finspong, Sweden: Siemens Industrial Turbomachinery AB, nd Print. 2018.

[32] Sayma A. Computational fluid dynamics. Bookboon; 2009.

[33] Anderson JD, Wendt J. Computational fluid dynamics. vol. 206. Springer; 1995.

[34] Versteeg HK, Malalasekera W. An introduction to computational fluid dynamics: the finite volume method. Pearson education; 2007.

[35] Davidson L, et al. Fluid mechanics, turbulent flow and turbulence modeling. Chalmers University of Technology, Goteborg, Sweden (Nov 2011). 2018.

[36] Jones WP, Launder BE. The prediction of laminarization with a two-equation model of turbulence. International journal of heat and mass transfer. 1972;15(2):301-14.

[37] Lardeau S, Billard F. Development of an elliptic-blending lag model for industrial applications. In: 54th AIAA Aerospace Sciences Meeting; 2016. p. 1600.

[38] Wilcox DC, et al. Turbulence modeling for CFD. vol. 2. DCW industries La Canada, CA; 1998.

[39] Puttkammer P. Boundary layer over a flat plate [B.S. thesis]. University of Twente; 2013.

[40] Reacting Flow;. Available from: https://docs.sw.siemens.com/documentation/external/PL20210401101005144/en-US/userManual/starccmp_userguide_html/index.html#page/STARCCMP%2FGUID-83013756-BBBE-4F7F-81B5-1C34D3023212.html%23. [cited 04.03.2022].

[41] Lindman O, Andersson M, Persson M, Munktell E. Development of a liquid fuel combustion system for SGT-750. In: Turbo Expo: Power for Land, Sea, and Air. vol. 45684. American Society of Mechanical Engineers; 2014. p. V04AT04A022.